METAMORPHIC HISTORY OF ECLOGITIC METAGABBRO BLOCKS FROM A TECTONIC MÉLANGE IN THE VOLTRI MASSIF, LIGURIAN ALPS, ITALY

Fraukje M. Brouwer*,, Reinoud L.M. Vissers*** and **William M. Lamb*****

* *Vening Meinesz Research School for Geodynamics, Faculty of Earth Sciences, Utrecht University, Postbus 80021, 3508 TA Utrecht, The Netherlands (Corresponding author. Present address: Institut für Geologie, Universität Bern, Baltzerstrasse 1, 3014 Bern, Switzerland. e-mail: brouwer@geo.unibe.ch)*

** *Geophysical Laboratory, Carnegie Institution of Washington, 5251 Broad Branch Road NW, Washington, DC 20015-1305, U.S.A.*

*** *Department of Geology and Geophysics, Texas A&M University, College Station, TX 77843-3115, U.S.A.*

Keywords: *thermal history, eclogites, mélange, Alpine, Voltri, Beigua.*

ABSTRACT

Iron/titanium-rich metagabbros, derived from the Beigua serpentinite unit, were collected from a tectonic mélange along the contact between the Beigua serpentinite unit and the underlying Voltri-Rossiglione calcschist unit of the Voltri Group in the Ligurian Alps of northern Italy. Petrographic study and microchemical analysis have been undertaken to unravel the details of their metamorphic history.

The metagabbros formed during Jurassic oceanisation in the Piedmont-Ligurian realm, and show local evidence of rodingitisation during ocean-floor metamorphism. Together with the country rock serpentinites, they were subjected to high-pressure metamorphism during Alpine subduction and eventual collision. The high-pressure assemblage in the metagabbro blocks consists of garnet, omphacite, glaucophane, and locally white mica, rutile or titanite. Peak metamorphic conditions, estimated using garnet-omphacite-phengite thermobarometry, were 500 ± 50°C and 17.5 ± 0.5 kbar, i.e. higher peak pressures than previously estimated for these rocks. The rocks cooled continuously during decompression. Exhumation initially proceeded along a low-$\Delta T/\Delta P$ trajectory, followed by final exhumation along a higher gradient close to that of a continental geotherm. The Voltri Massif had arrived at the Earth's surface by 34 million years ago, because exhumed rocks of the massif are covered by early Oligocene continental scree breccias and conglomerates.

We propose a combination of buoyancy of the serpentinites in the Beigua unit and corner flow in the orogenic wedge on top of the subducting Piedmont-Ligurian oceanic lithosphere as a plausible mechanism to drive exhumation of the high-pressure rocks of the Voltri Massif.

INTRODUCTION

Geology of the Voltri Massif

The Voltri Massif in the Ligurian Alps (Fig. 1) is the largest ophiolite massif in the Alps-Apennines system. The structure of the massif is dominated by sub-horizontal thrust sheets, affected by polyphase deformation and metamorphism. Three main units are commonly distinguished. From bottom to top: (1) the Voltri-Rossiglione calcschist unit consisting of blueschist to eclogite-facies calcareous metasediments, metavolcanics, and slices of serpentinite, (2) the Beigua serpentinite unit with heavily serpentinised ultramafics enclosing relatively small bodies of eclogitic metagabbro and locally metabasalt and, (3) the overlying lherzolite-dominated Erro-Tobbio peridotite. These units, also referred to as the Voltri Group, represent fragments of the subducted lithosphere of the Piedmont-Ligurian ocean, the Alps-Apennine part of the Mesozoic Tethys. This oceanic basin formed during Middle and Late Jurassic extension and was subject to intra-oceanic subduction and subsequent collision after the Early Cretaceous, leading to imbrication and stacking in the Alpine suture zone and emplacement of oceanic units onto the European continental crust. The bulk chemistry of the Beigua metagabbros indicates that they originated at a mid-oceanic ridge as tholeitic cumulates with MORB affinity. They were rodingitised at or near the seafloor before undergoing metamorphism at eclogite facies conditions during Alpine convergence. On the basis of outcrop and microscale overprinting relationships, a sequence of deformational structures has been determined in each thrust unit, which forms a basis for the relative timing of different metamorphic minerals and mineral assemblages in these units. All thrust units of the Voltri Group show an

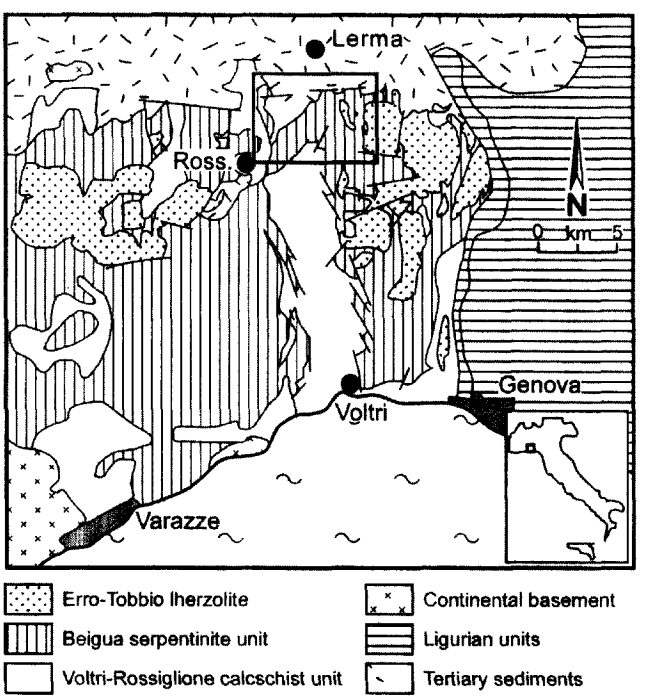

Fig. 1 - Location of the Voltri Massif, Italy, and sketch map of the Voltri Massif showing its large-scale structure (area outlined shown in Figure 2). Abbreviation: Ross.- Rossiglione.

eclogite, a blueschist-eclogite, and a greenschist-facies stage of deformation.

Tectonic mélange in the northern Voltri Massif

The rocks selected for this study are exposed in an area in the northern part of the Voltri Massif, SSE of the village of Lerma (Figs. 1, 2). Outcrop conditions in the region are generally poor due to dense vegetation, but the Piota riverbed (Fig. 2) provides excellent exposure in a domain where the contact of the Beigua serpentinite unit and the underlying Voltri-Rossiglione calcschist unit is subhorizontal. In the vicinity of the contact, the structure in the hanging-wall serpentinites is dominated by kink-type crenulations. Towards the base of the serpentinite unit these crenulations become more intense, and veins and patches of talc + chlorite + tremolite + carbonate replace the original antigorite-dominated assemblage. A layer of intensely foliated serpentine and actinolite-bearing talc-chlorite-tremolite-carbonate schist, at least several tens of metres thick, marks the thrust itself. This schistose material encloses rounded and lens-shaped (phacoid) blocks of eclogitic Fe-Ti and Mg gabbro that are up to 20 metres across (Fig. 3), blocks of greenschist-facies and occasionally eclogitic metabasalt, blocks of massive and foliated serpentinite, and lenses and blocks of calcschist and calcareous marble. On the basis of its structural features this chaotic lithology has been interpreted as a tectonic mélange. Comparison of the structures and metamorphic mineral assemblages in the wall rock units with those in the mélange indicates that the mélange formed during a late stage of ductile thrusting under greenschist facies conditions. The blocks and lenses probably developed during localised deformation in a relatively narrow zone, up to several tens of metres thick, along the thrust. An overall top-to-the-NW movement sense is inferred on the basis of shear zone geometries and asymmetric extensional crenula-

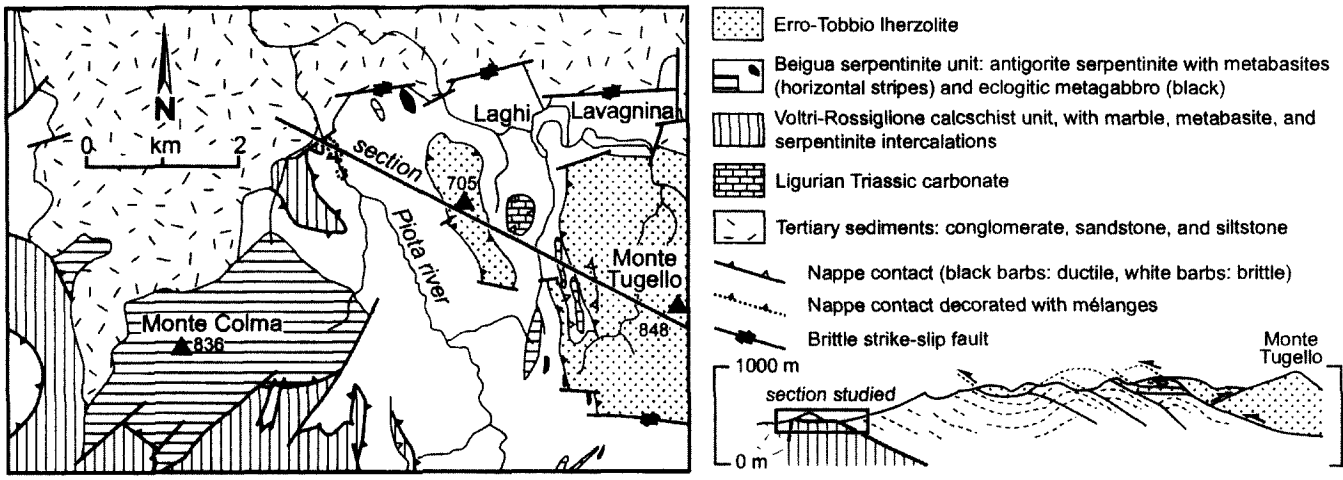

Fig. 2 - Sketch map and cross section of the central northern Voltri Massif south of the village of Lerma, showing location of mélange exposures in the Piota riverbed.

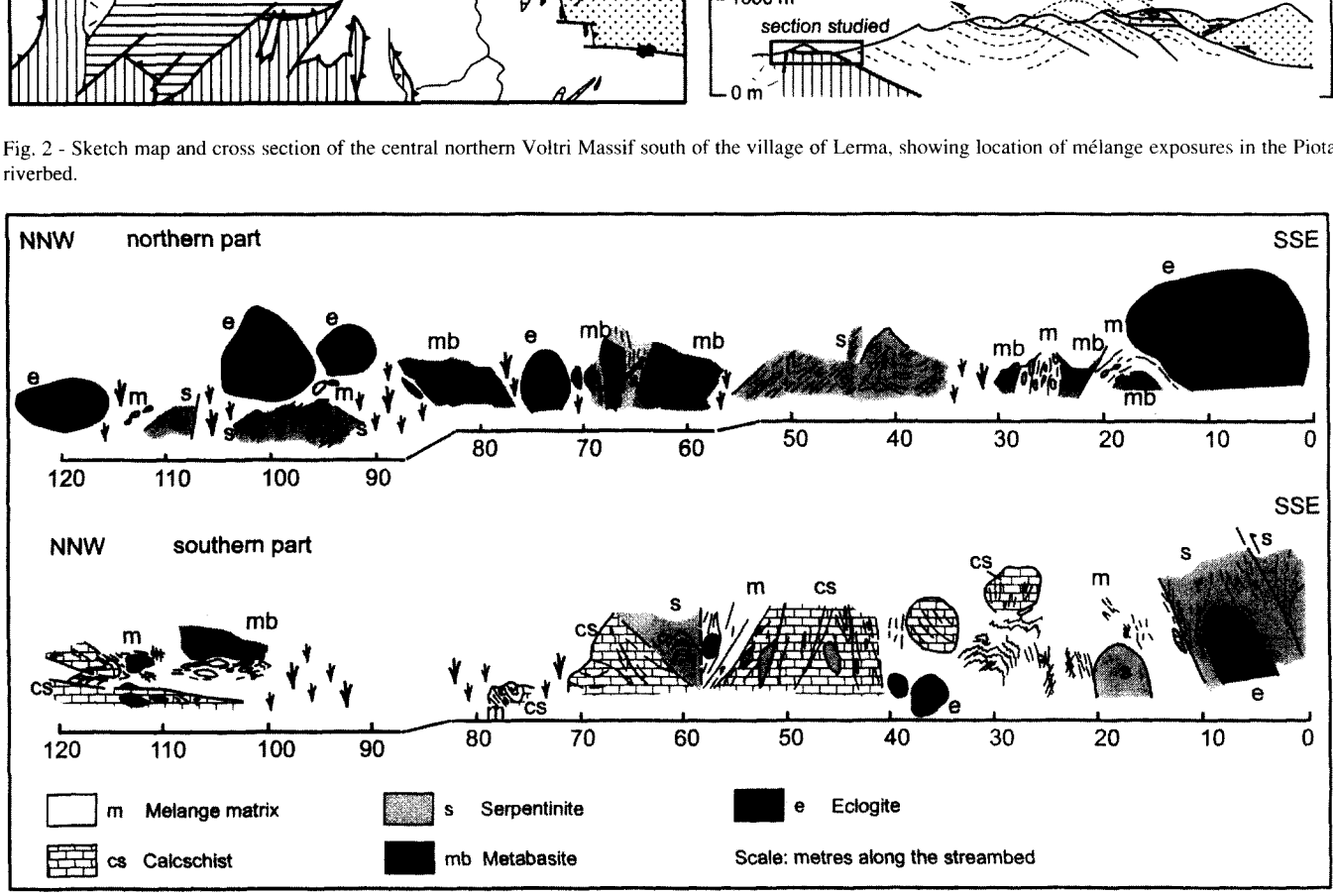

Fig. 3 - Detailed section across part of the mélange exposure in the Piota riverbed.

tion cleavages in the mélange matrix, in combination with the orientations of stretching fabrics and long axes of elongate lens-shaped blocks.

The most striking feature of the mélange is the occurrence of rounded blocks of eclogitic metagabbro (Figs. 3, 4a), up to some 20 meters in diameter. Where erosion has provided sections across such blocks, they consistently show eclogitic cores, often with flaser microstructures and locally with fine-grained mylonitic fabrics, and dm-scale retrogressed rims (Fig. 4b). The mineral assemblages seen in the cores of the blocks are identical to those in eclogitic metagabbros in the Beigua serpentinite unit, and allow identification of a stage of HP metamorphism. The rims of the blocks are strongly retrogressed and contain actinolite, grown at the expense of blue-green amphibole, in the presence of albite, chlorite, epidote, titanite, magnetite and pyrite, while at the contact with the mélange matrix the assemblage may contain Mg-chlorite plus tremolite. These retrogressive rims are discordant to the eclogitic flaser structure in the cores of the blocks, indicating that retrogression and mélange formation post-date the flaser layering. The internal parts of the retrogressive rims may show static assemblages with little evidence of deformation, while in the outer few centimetres the rims often show a distinct foliation parallel to the main fabric of the mélange matrix.

We performed a detailed petrographical and microchemical study of 32 samples taken from 9 metagabbro blocks. In order to constrain the retrograde metamorphic history of the rocks, we selected our samples to optimally cover their variable degree of retrograde metamorphism.

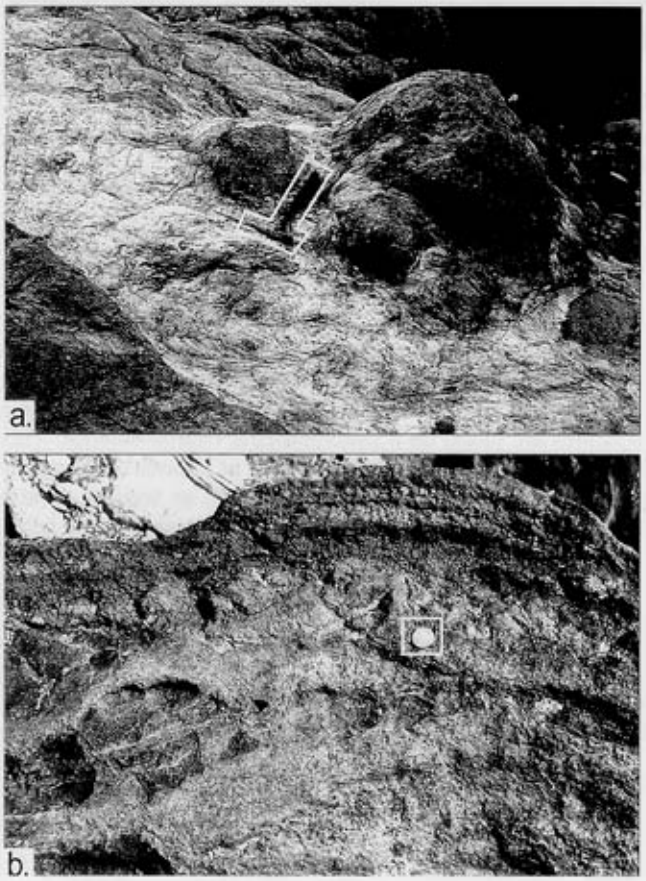

Fig. 4 - Field aspects of the tectonic mélange. a. Rounded metagabbro blocks in talc-chlorite-tremolite-carbonate schist; hammer for scale. b. Retrogressed rim developed in an eclogitic metagabbro block; coin for scale (diameter 1.5 cm).

Metagabbros of the Voltri mélange

The mineral abbreviations used in the following sections are taken from Kretz. In addition, WhM is used to denote unspecified white mica, while Carb refers to unspecified carbonate minerals, and Op to opaque minerals.

Petrography

The cores of the metagabbro blocks from the Voltri mélange often show a high-pressure metamorphic mineral assemblage with garnet, omphacite, and glaucophane crystals and aggregates up to several millimetres across. Towards the rims of the blocks, these high-pressure minerals are gradually replaced by darker amphiboles, such that the retrograde rims show darker colours than the relatively unaltered eclogitic cores (Fig. 4b).

The successive mineral assemblages of the metagabbros are listed in Figure 5. The high-pressure metamorphic mineral assemblage of the metagabbros is dominated by euhedral garnet crystals, large (up to 5 mm in diameter) omphacites and glaucophane (Fig. 6a). The large omphacites have pressure shadows of finer-grained omphacite and glaucophane (Fig. 6b). The cores of large omphacites locally show exsolution of iron-rich talc, which, although they occur within high-pressure omphacites, likely result from retrogressive breakdown of the pyroxene (Nisio and Lardeaux, 1987). Talc does not occur outside omphacite and is therefor not considered a product of prograde or peak metamorphism. Small white mica crystals are locally enclosed in omphacite. Glaucophane, rutile, titanite, quartz, and white mica constitute the inclusion population within garnet, while lozenge-shaped aggregates of clinozoisite + plagioclase suggest breakdown of precursor lawsonite (Fig. 6c). Minor quantities of quartz are present in some of our samples. In some samples white mica, rutile, or titanite is part of the high-pressure assemblage, although rutile and titanite do not coexist in any of the samples. Omphacite locally shows thin symplectitic rims developed during retrograde metamorphism. In other samples glaucophane, and later blue-green amphibole and plagioclase developed at the expense of omphacite. Glaucophanes are often rimmed by barroisitic amphiboles and locally have an outer rim of actinolite (Fig. 6d). In some places these zoned amphiboles have a symplectitic rim of green amphibole (actinolite?) and plagioclase (symplectite 2 of Messiga and Scambelluri, 1991). Cli-

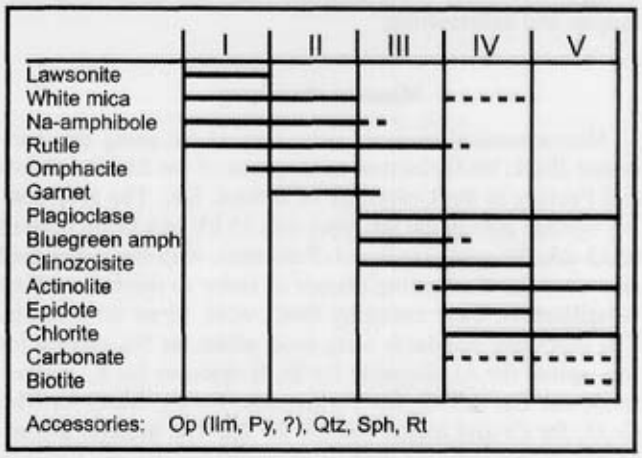

Fig. 5 - Mineral assemblages of the metagabbro blocks. Dashed lines: present in some but not all of the studied samples.

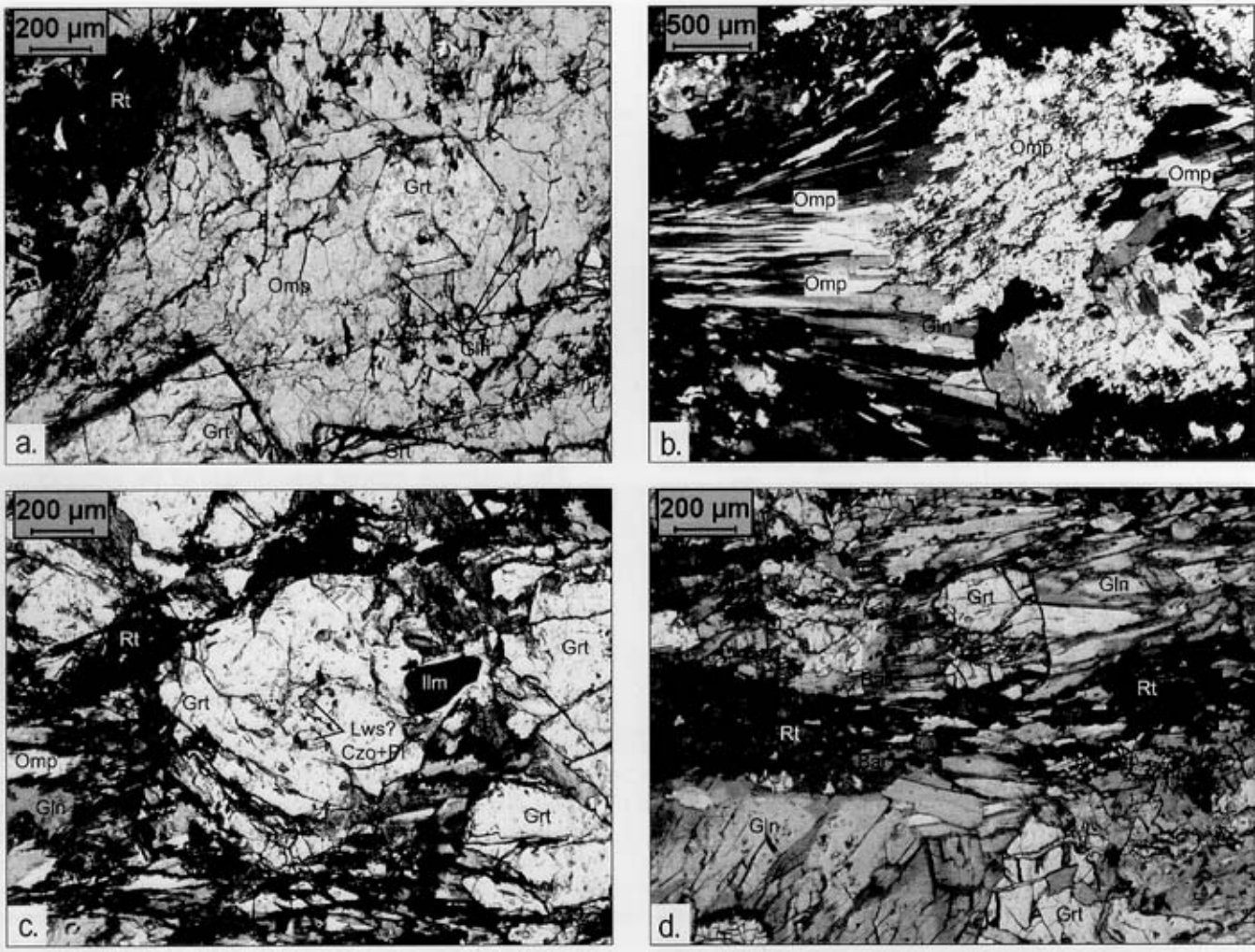

Fig. 6 - Petrography of the metagabbro blocks. a. Garnet, omphacite and glaucophane are the main constituents of the high-pressure mineral assemblage. b. Large omphacites, with smaller omphacites and glaucophane in pressure shadow. Large omphacite (light colour) contains exsolutions of talc. c. Inclusions of clinozoisite and plagioclase, possibly pseudomorphic after lawsonite, within garnet. d. Glaucophane breakdown to barroisite and barroisite breakdown to actinolite.

nozoisite, and later epidote and some plagioclase often replace garnet. The later stages of retrogression involve the formation of large quantities of chlorite at the expense of garnet. In samples from the retrograde rims of metagabbro blocks, minor quantities of biotite occur at the rims of chlorite crystals. The occurrence of biotite, as well as the presence of some carbonate probably reflects extensive fluid activity and possibly some metasomatism during mélange formation and deformation.

Mineral chemistry

Microchemical analyses were carried out using the automated JEOL 8600 electron microprobe of the EU Geochemical Facility at the University of Bristol, UK. The accelerating voltage during the analyses was 15 kV at a beam current of 15 nA, the spot size was 1-5 microns, with the larger spot size used for Na-bearing phases in order to minimise alkali volatilisation. Peak counting times were 15 or 20 seconds. The following standards were used: albite for Na, olivine for Mg, spinel for Al, diopside for Si, K-feldspar for K, wollastonite for Ca, $SrTiO_3$ for Ti, hematite for Fe, MnO for Mn, Cr_2O_3 for Cr and nickel (metal) for Ni. The mineral assemblages of the samples studied microchemically are listed in Table 1. Representative analyses of Grt, Omp, amphiboles, Ep, Pl, WhM, Bt, and Chl are listed in Table 2.

Ferric iron estimation

Accurate determination of the relative proportions of ferric (trivalent) and ferrous (divalent) iron by electron microprobe analysis is extremely difficult. Various workers have therefore proposed recalculation schemes to estimate the ferric iron content of silicate minerals. Most of these schemes are based on a stoichiometric charge balance. This approach assumes, that if the number of cations of the recalculated mineral formula, taking all iron as ferrous, is less than stoichiometric, this is caused by the presence of ferric iron. Alternatively, for the case of clinopyroxene, recalculation schemes have been proposed that only allocate ferric iron if there is an excess of Na over Al.

Following earlier work, a mixed approach has been

Table 1 - Mineral assemblages of samples studied.

SAMPLE	MAIN	INCL / EARLY	RIMS / LATE	ACCESSORIES
MEL96-1B	Gln, Grt, Omp	Ep	Amph, Chl (later), Czo, Pl	Op, Pl, Py, Qtz, Rt, Tln
MEL96-1E	Gln, Grt, Omp, Tln	Gln, Omp, WhM	Amph, Bt, Ep, Pl	Pl, Py, Qtz, Tln
MEL96-2B	Gln, Grt, Omp, WhM		Amph	Pl, Py, Qtz, Tln
MEL96-3A	Gln, Grt, Omp		Chl, Ep, Pl	Op, Pl, Py, Qtz, Rt, Tln
MEL96-4B	Gln, Grt, Omp, WhM	Czo, Gln, WhM	Amph, Chl, Ep	Pl, Py, Qtz, Tln
MEL96-4c	Czo, Gln, Grt, Omp, WhM		Amph, Chl, Ep	Op, Pl, Py, Qtz, Tln
MEL96-4d	Gln, Grt, Omp	Czo, Gln, WhM	Amph, Bt, Chl, Pl	Op, Pl, Py, Qtz, Tln
MEL96-4G	Amph, Carb, Chl, Pl, WhM			Apt,
MEL96-9A	Gln, Grt, Omp, WhM		Amph, Ep, Pl, WhM	Carb, Pl, Py, Qtz, Tln

Mineral abbreviations taken from Kretz, Amph denotes blue-green or green amphibole.

adopted here for recalculation of mineral analyses to estimate the amounts of trivalent iron. Ferric iron in garnet is estimated using Droop's (1987) charge balance equation, while for clinopyroxene we applied the method of Cawthorn and Collerson. Amphiboles were recalculated according to charge balance as described by Holland and Blundy, and the ferric iron content in biotite was estimated from the hematite content of coexisting ilmenite. The latter calculation was done for a few pairs and all other biotites were assumed to contain similar amounts of Fe^{3+}. All other minerals have been assumed to contain ferrous iron only, either because they contain only minor amounts of iron (e.g. feldspars), or because estimation by means of charge balance would be very inaccurate, as in the case of white mica, where the water content is unknown.

Garnet

Garnet compositions are fairly similar for all analysed metagabbro samples (Fig. 7a). The garnets analysed have a compositional range of $Alm_{60-75}And_{4-10}Grs_{12-25}Prp_{2-15}Sps_{1-15}$, and they are often strongly zoned with respect to their iron, magnesium and manganese contents (Fig. 8a-d). Garnets cores are locally very rich in manganese (Sps_{25-40}) and much poorer in iron (Alm_{35-50}) than the average garnet. The relative proportions of iron and magnesium are indicative of the temperature during garnet formation. The low-magnesium garnet composition, as well as the presence of substantial amounts of rutile as part of the high-pressure mineral assemblage, indicates that all of our samples were originally Fe-Ti gabbros, rather than Mg-gabbros.

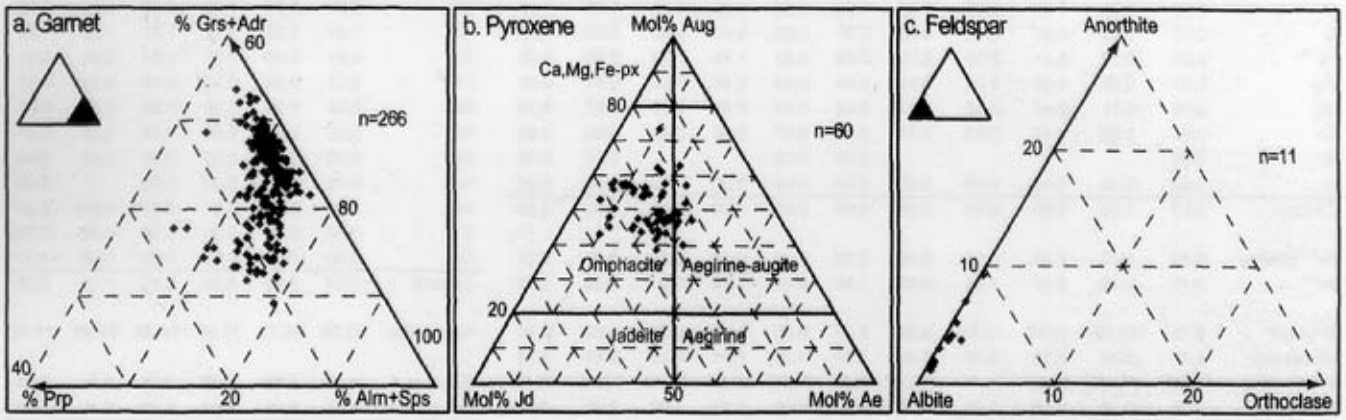

Fig. 7 - Mineral compositions for the metagabbro blocks. a. Garnet compositions. b. Clinopyroxene compositions. c. Plagioclase compositions.

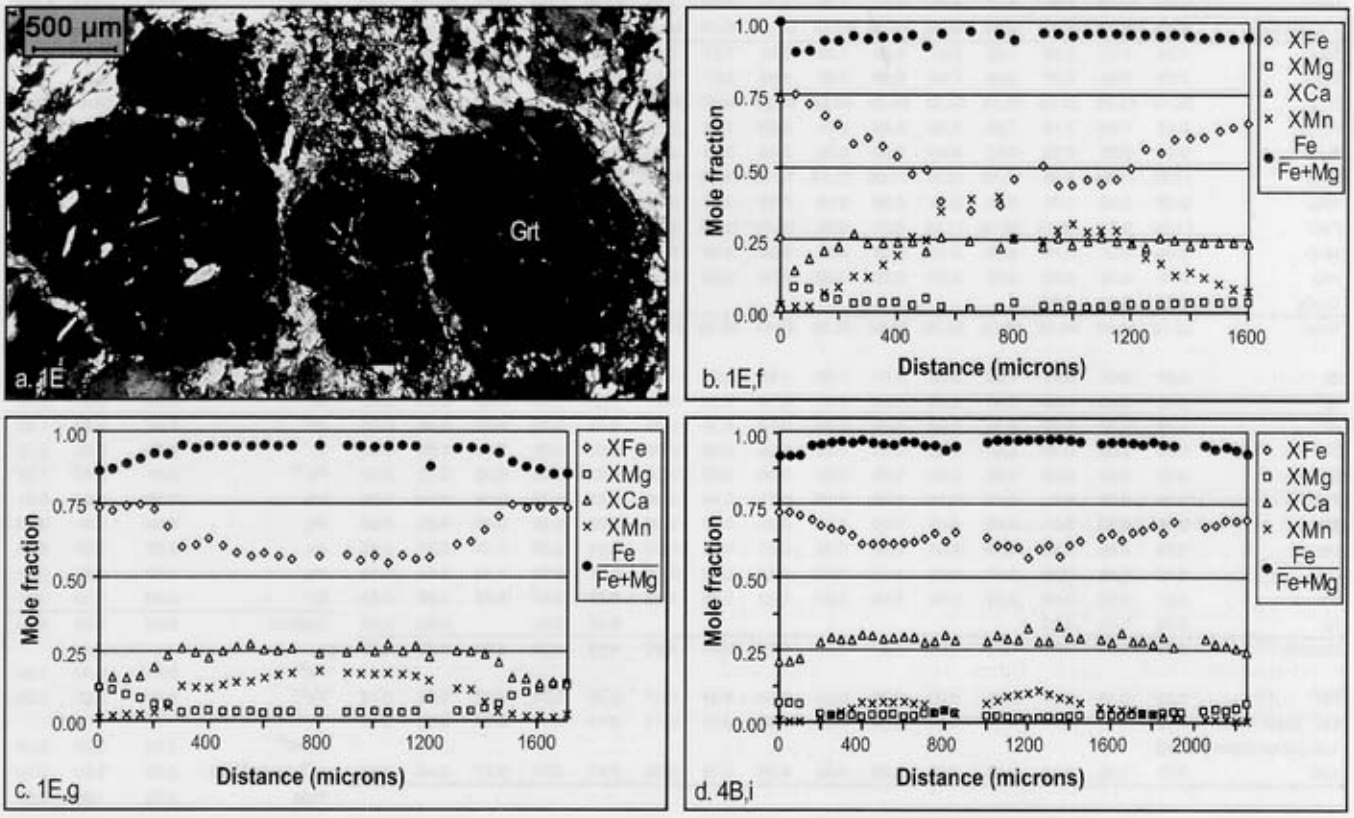

Fig. 8 - Garnet zoning in metagabbro blocks. a. Photomicrograph of a zoned metagabbro garnet from sample MEL96-1E. b. Compositional variation across a zoned metagabbro garnet. c. Id. d. Id.

Table 2 - Representative analyses of different minerals in wt%.

Mineral	Grt	Grt	Grt	Grt	Grt	Grt	Grt	Grt	Grt	Grt	Grt
Point	3.108	3.16	4.56	4.75	3.32	3.155	3.161	2.6	2.29	2.99	2.100
Thin section	96-1B	96-1E	96-	96-3A	96-	96-4c	96-4c	96-	96-	96-9A	96-
Na_2O	0.03	0.07	0.02	0.03	0.00	0.06	0.00	0.04	0.00	0.02	0.04
MgO	2.31	2.64	3.46	4.17	1.38	0.52	2.00	0.43	1.66	1.41	1.50
SiO_2	37.45	36.82	37.25	37.34	36.67	37.19	37.23	36.41	36.43	37.32	37.14
Al_2O_3	20.14	21.03	21.16	21.03	20.87	19.93	20.31	20.25	20.77	20.33	20.13
K_2O	0.01	0.02	0.01	0.00	0.00	0.00	0.00	0.00	0.01	0.00	0.00
CaO	6.33	4.55	5.46	6.26	8.28	9.95	6.67	10.32	7.59	6.99	7.18
TiO_2	0.04	0.00	0.04	0.03	0.07	0.05	0.06	0.19	0.05	0.03	0.06
FeO	33.80	34.72	31.49	30.95	31.86	30.87	33.14	25.43	32.61	33.95	33.30
MnO	0.22	0.70	0.53	0.36	0.16	1.33	0.48	6.37	0.23	0.07	0.36
Cr_2O_3	0.00	0.03	0.00	0.00	0.06	0.05	0.00	0.07	0.01	0.00	0.07
NiO	0.00					0.00	0.00			0.01	0.00
Total	100.25	100.45	99.39	100.12	99.29	99.91	99.89	99.47	99.33	100.01	99.66
Si	3.00	2.94	2.98	2.95	2.96	3.00	2.99	2.95	2.94	3.00	3.00
Al	1.90	1.98	1.99	1.96	1.99	1.90	1.93	1.93	1.98	1.93	1.92
Ti	0.00	0.00	0.00	0.00	0.00	0.00	0.00	0.01	0.00	0.00	0.00
Fe^{tot}	2.26	2.32	2.11	2.04	2.15	2.08	2.23	1.72	2.20	2.29	2.25
Mn	0.01	0.05	0.04	0.02	0.01	0.09	0.03	0.44	0.02	0.01	0.02
Mg	0.28	0.31	0.41	0.49	0.17	0.06	0.24	0.05	0.20	0.17	0.18
Ca	0.54	0.39	0.47	0.53	0.72	0.86	0.57	0.89	0.66	0.60	0.62
Ni	0.00					0.00	0.00			0.00	0.00
Cr	0.00	0.00	0.00	0.00	0.00	0.00	0.00	0.00	0.00	0.00	0.00
Cations	8.00	8.00	8.00	8.00	8.00	8.00	8.00	8.00	8.00	8.00	8.00
Fe^{3+} (Droop)	0.10	0.13	0.04	0.14	0.08	0.09	0.08	0.14	0.13	0.06	0.07
Fe^{2+}	2.17	2.19	2.07	1.91	2.07	1.99	2.15	1.58	2.07	2.23	2.18
XPyrope	9.18	10.69	13.85	16.64	5.60	2.07	8.00	1.75	6.77	5.63	5.99
XAndradite	4.91	6.08	2.15	6.68	4.06	4.79	4.08	7.51	6.25	2.95	3.79
XAlmandine	72.24	74.48	69.26	64.59	69.87	66.26	71.74	53.27	70.40	74.14	72.50
XUvarovite	0.00	0.09	0.00	0.00	0.17	0.16	0.00	0.23	0.03	0.00	0.22
XSpessartine	0.50	1.60	1.19	0.82	0.36	3.03	1.09	14.75	0.52	0.17	0.81
XGrossular	13.17	7.07	13.55	11.27	19.94	23.69	15.08	22.49	16.03	17.10	16.69

Mineral	WhM	WhM	WhM	WhM	WhM	WhM
Point	3.156	3.160	3.162	3.163	2.7	2.96
Thin	96-4c	96-4c	96-4c	96-4c	96-	96-
Na_2O	0.36	0.04	0.11	0.11	0.00	0.03
MgO	2.78	5.33	5.53	5.55	5.09	5.03
SiO_2	49.54	55.63	55.77	55.67	52.25	53.84
Al_2O_3	26.93	20.15	21.15	21.03	20.01	19.92
K_2O	10.67	11.07	10.70	10.46	10.13	11.01
CaO	0.00	0.00	0.02	0.03	0.14	0.01
TiO_2	0.12	0.07	0.14	0.13	0.11	0.10
FeO	4.69	4.32	3.01	3.32	5.33	3.58
MnO	0.04	0.01	0.00	0.04	0.03	0.09
Cr_2O_3	0.01	0.06	0.00	0.00	0.00	0.07
NiO	0.00	0.00	0.02	0.00		0.00
Total	95.09	96.63	96.41	96.29	93.07	93.57
Si	3.36	3.69	3.68	3.68	3.62	3.68
Al^{IV}	0.64	0.31	0.32	0.32	0.38	0.32
Al^{VI}	1.51	1.27	1.32	1.31	1.26	1.29
Ti	0.01	0.00	0.01	0.01	0.01	0.01
Fe^{tot}	0.27	0.24	0.17	0.18	0.31	0.21
Mn	0.00	0.00	0.00	0.00	0.00	0.01
Mg	0.28	0.53	0.54	0.55	0.53	0.51
Ca	0.00	0.00	0.00	0.00	0.01	0.00
Ni	0.00	0.00	0.00	0.00		0.00
Na	0.05	0.01	0.01	0.01	0.00	0.00
K	0.92	0.94	0.90	0.88	0.90	0.96
Cr	0.00	0.00	0.00	0.00	0.00	0.00
Cations	7.04	6.99	6.95	6.95	7.00	6.99
Mg-number	51.39	68.71	76.61	74.88	62.99	71.45
Si (p.f.u.)	3.36	3.69	3.68	3.68	3.62	3.68
Oct (p.f.u.)	2.07	2.04	2.04	2.05	2.10	2.02

Mineral	Cpx	Cpx	Cpx	Cpx	Cpx	Cpx	Cpx	Cpx	Cpx	Cpx	Cpx	Cpx	Cpx	Cpx	Cpx
Point	3.107	3.105	2.80	3.17	4.55	4.64	4.72	4.74	3.30	3.33	3.159	3.164	2.28	2.102	2.103
Thin section	96-1B	96-1B	96-1E	96-1E	96-2B	96-2B	96-3A	96-3A	96-4B	96-4B	96-4c	96-4c	96-4d	96-9A	96-9A
Na_2O	7.24	7.50	8.69	7.42	6.51	8.03	7.98	7.41	7.87	6.42	8.21	6.72	7.76	7.90	7.97
MgO	7.09	7.05	5.07	6.06	7.50	6.86	6.97	7.66	6.37	7.27	6.31	7.32	6.63	6.56	5.88
SiO_2	55.14	55.68	55.06	53.76	54.59	55.39	54.59	54.83	54.67	54.13	56.07	55.75	54.18	56.13	55.80
Al_2O_3	6.43	7.60	7.16	7.08	6.10	8.25	8.04	6.93	7.56	7.09	10.48	8.87	7.51	9.37	8.24
K_2O	0.00	0.00	0.00	0.00	0.00	0.00	0.02	0.03	0.00	0.00	0.00	0.00	0.02	0.00	0.01
CaO	12.00	11.94	9.08	11.48	13.37	11.00	11.16	12.43	10.98	13.92	10.90	13.30	11.75	11.44	11.15
TiO_2	0.00	0.00	0.01	0.05	0.04	0.00	0.16	0.10	0.02	0.00	0.00	0.02	0.06	0.02	0.06
FeO	11.20	9.74	13.43	12.18	11.12	9.31	9.69	10.25	10.95	9.76	7.11	7.28	11.12	7.89	10.76
MnO	0.06	0.00	0.16	0.08	0.10	0.00	0.03	0.00	0.00	0.00	0.00	0.00	0.11	0.00	0.15
NiO	0.03	0.00	0.00	0.02	0.00	0.00	0.00	0.00	0.00	0.10	0.00	0.03	0.02	0.05	0.03
Cr_2O_3	0.04	0.00	0.00								0.01	0.00		0.06	0.00
Total	99.10	99.52	98.66	98.02	99.30	98.84	98.59	99.64	98.39	98.69	99.09	99.24	99.12	99.29	99.99
Si	2.01	2.01	2.02	1.99	2.00	2.01	1.98	1.98	2.00	1.99	2.01	2.02	1.97	2.02	2.01
Al^{IV}	0.00	0.00	0.00	0.01	0.00	0.00	0.02	0.02	0.00	0.01	0.00	0.00	0.03	0.00	0.00
Al^{VI}	0.28	0.32	0.31	0.30	0.26	0.35	0.33	0.28	0.33	0.29	0.44	0.38	0.29	0.40	0.35
Ti	0.00	0.00	0.00	0.00	0.00	0.00	0.00	0.00	0.00	0.00	0.00	0.00	0.00	0.00	0.00
Cr	0.00	0.00	0.00	0.00	0.00	0.00	0.00	0.00	0.00	0.00	0.00	0.00	0.00	0.00	0.00
Fe^{tot}	0.34	0.29	0.41	0.38	0.34	0.28	0.29	0.31	0.34	0.30	0.21	0.22	0.34	0.24	0.32
Mg	0.00	0.00	0.01	0.00	0.00	0.00	0.00	0.00	0.00	0.00	0.00	0.00	0.00	0.00	0.00
Mn	0.39	0.38	0.28	0.33	0.41	0.37	0.38	0.41	0.35	0.40	0.34	0.39	0.36	0.35	0.32
Ca	0.47	0.46	0.36	0.46	0.52	0.43	0.43	0.48	0.43	0.55	0.42	0.52	0.46	0.44	0.43
Na	0.51	0.53	0.62	0.53	0.46	0.56	0.56	0.52	0.56	0.46	0.57	0.47	0.55	0.55	0.56
Ni	0.00	0.00	0.00								0.00	0.00		0.00	0.00
Cations	4.00	4.00	4.00	4.00	4.00	4.00	4.00	4.00	4.00	4.00	4.00	4.00	4.00	4.00	4.00
Fe^{3+}	0.21	0.18	0.27	0.24	0.20	0.20	0.24	0.26	0.23	0.17	0.10	0.06	0.28	0.12	0.18
Fe^{2+} (C&C 1974)	0.13	0.12	0.14	0.13	0.14	0.08	0.05	0.05	0.11	0.13	0.11	0.17	0.06	0.12	0.15
XJd (=Xna-Xacm (Fe3+))															
XJd	0.30	0.35	0.35	0.29	0.26	0.36	0.32	0.26	0.33	0.29	0.47	0.42	0.27	0.43	0.38

Mineral	Ep	Ep	Ep
Point	4.12	2.515	3.169
Thin section	96-3A	96-4B	96-4c
Na_2O	0.00	0.06	0.03
MgO	0.00	0.06	0.01
SiO_2	38.10	38.41	36.96
Al_2O_3	25.03	28.94	20.00
K_2O	0.01	0.02	0.00
CaO	23.84	23.55	23.34
TiO_2	0.06	0.07	0.00
FeO	9.27	6.42	15.28
MnO	0.07	0.22	0.10
Cr_2O_3	0.01	0.08	0.00
NiO	0.08		0.00
Total	96.30	97.69	95.68
Si	3.02	2.97	3.00
Al^{IV}	0.00	0.03	0.00
Al^{VI}	2.34	2.60	1.92
Ti	0.00	0.00	0.00
Fe^{tot}	0.61	0.40	1.04
Mn	0.00	0.01	0.01
Mg	0.00	0.01	0.00
Ca	2.02	1.95	2.03
Na	0.00	0.01	0.01
Cr	0.00	0.00	0.00
Cations	8.00	7.98	8.00
Fe^{3+}	0.61	0.40	1.04
Fe^{2+}	0.00	0.00	0.00
$Si+Al^{IV}$	3.02	3.00	3.00
$Al^{VI}+Ti+Fe^{3+}+Cr$	2.95	3.00	2.95
Rest	2.03	1.98	2.04

Mineral	Bt	Bt	Bt	Bt
Point	2.416	2.426	1.457	1.465
Thin section	96-1E	96-1E	96-4d	96-4d
Na_2O	0.62	0.09	0.10	0.16
MgO	1.63	11.67	4.67	9.01
SiO_2	44.97	36.11	34.01	35.74
Al_2O_3	27.42	16.87	15.71	15.56
K_2O	9.28	9.61	6.33	5.19
CaO	0.35	0.06	2.51	0.51
TiO_2	0.44	0.32	0.59	0.41
FeO	7.48	19.30	29.04	25.63
MnO	0.10	0.56	0.70	0.37
Cr_2O_3	0.01	0.05	0.00	0.00
NiO				
Total	92.29	94.60	93.65	92.57
Si	3.20	2.78	2.76	2.83
Al^{IV}	0.80	1.22	1.24	1.17
Al^{VI}	1.49	0.31	0.27	0.29
Ti	0.02	0.02	0.04	0.02
Fe^{tot}	0.44	1.24	1.97	1.70
Mn	0.01	0.04	0.05	0.02
Mg	0.17	1.34	0.57	1.06
Ca	0.03	0.00	0.22	0.04
Ni				
Na	0.09	0.01	0.02	0.03
K	0.84	0.94	0.86	0.53
Cr	0.00	0.00	0.00	0.00
Cations	7.09	7.91	7.78	7.69
Fe^{3+}	0.07	0.19	0.30	0.25
Fe^{2+}	0.38	1.06	1.68	1.44
XAl	0.72	0.11	0.10	0.10
XTi	0.01	0.01	0.01	0.01

Mineral	Amp	Amp	Amp	Amp
Point	3.103	4.212	4.15	4.39
Thin section	96-1B	96-1E	96-3A	96-4G
Na_2O	6.74	4.22	2.75	0.35
MgO	9.47	9.12	8.71	21.20
SiO_2	57.22	48.58	46.65	57.77
Al_2O_3	7.48	7.29	7.27	0.08
K_2O	0.03	0.30	0.21	0.02
CaO	0.62	9.06	9.63	12.94
TiO_2	0.00	0.00	0.25	0.00
FeO	14.66	18.07	21.52	5.11
MnO	0.11	0.10	0.18	0.21
Cr_2O_3	0.00	0.05	0.05	0.03
NiO	0.03	0.05	0.06	0.06
Total	96.33	96.73	97.16	97.65
Si	8.04	7.31	7.11	7.99
Al^{IV}	0.00	0.69	0.86	0.01
Al^{VI}	1.24	0.60	0.44	0.01
Ti	0.00	0.00	0.03	0.00
Fe^{tot}	1.72	2.27	2.74	0.59
Mn	0.01	0.01	0.02	0.02
Mg	1.98	2.04	1.98	4.37
Ca	0.09	1.46	1.57	1.92
Ni	0.00	0.01	0.01	0.01
Na	1.84	1.23	0.81	0.09
K	0.01	0.06	0.04	0.00
Cr	0.00	0.00	0.00	0.00
Cations	14.93	15.68	15.63	15.02
Fe^{3+}	0.66	0.00	0.00	0.06
Fe^{2+}	1.07	2.27	2.74	0.54

Mineral	Chl	Chl	Chl	Chl
Point	4.70	1.112	1.472	4.47
Thin section	96-3A	96-4B	96-4d	96-4G
Na_2O	0.02	0.02	0.34	0.02
MgO	13.51	13.67	13.22	26.87
SiO_2	25.06	26.46	27.11	30.34
Al_2O_3	18.74	17.08	16.77	15.12
K_2O	0.00	0.00	0.05	0.00
CaO	0.03	0.08	0.72	0.00
TiO_2	0.00	0.00	0.05	0.00
FeO	29.09	28.99	27.41	11.20
MnO	0.16	0.21	0.37	0.21
Cr_2O_3	0.00	0.08	0.06	0.78
NiO		0.00		0.00
Total	86.59	86.49	86.04	84.52
Si	5.49	5.78	5.93	6.16
Al^{IV}	2.51	2.22	2.07	1.84
Al^{VI}	2.32	2.18	2.25	1.77
Ti	0.00	0.00	0.01	0.00
Fe^{tot}	5.33	5.30	5.01	1.90
Mn	0.03	0.04	0.07	0.04
Mg	4.41	4.45	4.31	8.13
Ca	0.01	0.02	0.17	0.00
Ni		0.00		0.00
Na	0.01	0.01	0.14	0.01
Cr	0.00	0.01	0.01	0.12
OH	16.00	16.00	16.00	16.00
Cations	36.10	36.01	35.97	35.98

Mineral	Pl	Pl	Pl	Pl
Point	4.251	4.4	1.111	4.18
Thin section	96-1E	96-3A	96-4B	96-4d
Na_2O	10.55	11.41	10.87	11.76
MgO	1.50	0.01	0.00	0.00
SiO_2	66.38	68.07	66.76	68.47
Al_2O_3	17.79	19.60	20.22	19.03
K_2O	0.06	0.02	0.02	0.06
CaO	1.96	0.62	1.11	0.24
TiO_2	0.06	0.00	0.00	0.00
FeO	1.59	0.20	0.26	0.12
MnO	0.00	0.02	0.00	0.06
Cr_2O_3	0.00	0.00	0.00	0.06
NiO	0.01	0.02	0.01	0.02
Total	99.89	99.90	99.24	99.68
Si	3.02	2.99	2.96	3.00
Al	0.95	1.01	1.06	0.98
Ca	0.10	0.03	0.05	0.01
Na	0.93	0.97	0.93	1.00
K	0.00	0.00	0.00	0.00
Cations	5.00	5.00	5.00	5.00
X_{Ab}	0.90	0.97	0.95	0.99
X_{An}	0.09	0.03	0.05	0.01
X_{Or}	0.00	0.00	0.00	0.00

All sample codes start with MEL. Garnet analyses recalculated to 12 oxygens and 8 cations; pyroxene analyses normalised to 6 oxygens and 4 cations; plagioclase analyses normalised to 5 cations; epidote group mineral analyses recalculated to 12.5 oxygens and 8 cations; mica analyses recalculated to 11 oxygens; and chlorite analyses recalculated to 28 oxygens and 16 OH-groups.

Clinopyroxene

The composition of pyroxenes analysed is shown in the ternary diagram of Figure 7b. The nomenclature used for sodic-calcic pyroxenes is adapted from Morimoto et al.. Jadeite contents were calculated as the sodium content minus the amount of acmite. Most pyroxene analyses plot within the omphacite field, although some aegirine-augites with compositions close to the omphacite field have been found as well.

Amphibole

The optical observation that amphiboles in the metagabbros show a large compositional variation is confirmed by microchemical analyses. Following the nomenclature of Leake, the amphiboles analysed are subdivided in four different groups. The alkali amphiboles are related to high-pressure metamorphism, and they have the composition of glaucophanes or ferro-glaucophanes, locally ranging to crossite (Fig. 9a). Sodic amphiboles mostly plot in the ferro-winchite field (Fig. 9b). The pargasitic amphiboles are mostly ferro-edenites and locally silicic ferro-edenites (Fig. 9c), tschermakitic amphiboles are mostly actinolite and sometimes ferro-actinolite (Fig. 9d).

Feldspar

The few feldspar crystals analysed cluster near the pure albite endmember (Fig. 7c). The maximum analysed anorthite content is almost 10%, whereas a maximum of 3% orthoclase component has been found.

White mica

White micas were only analysed in a few samples (Fig. 10). The white micas generally have a very high Si content, with up to 3.68 Si per formula unit. The high Si content of the white micas indicates that they crystallised at high pressures.

METAMORPHIC HISTORY

Thermobarometry

The metagabbro samples show evidence of high-pressure metamorphism, followed by several retrograde mineral transformations. This implies that they preserve at least a partial record of evolving pressure-temperature conditions. Deciphering the pressure-temperature record is challenging because of the difficulty in demonstrating that a given assemblages has preserved equilibrium mineral compositions during changing pressure-temperature conditions. The preservation of partial retrogression and mineral zonation demonstrate the need for caution when one attempts to quantify metamorphic temperatures and pressures using the compositions of co-existing minerals. However, careful examination of textures and microstructures permits selection of mineral pairs most suitable for geothermobarometry. The

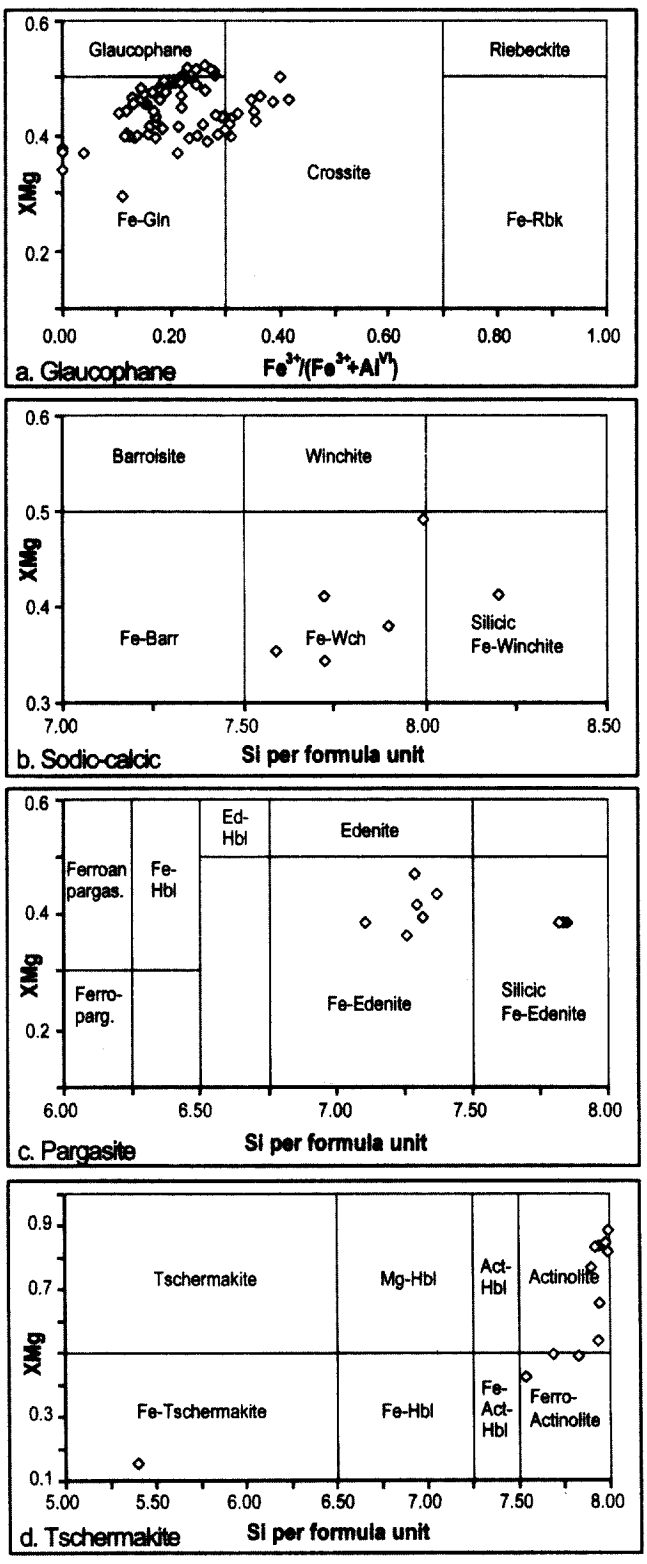

Fig. 9 - Amphibole compositions. a. Alkali amphiboles, glaucophane series. b. Sodic-calcic amphiboles. c. Calcic amphiboles, pargasite series. d. Calcic amphiboles, tschermakite series.

exact formulations of thermobarometric calibrations used in this study are summarised in the appendix. Provided that the microprobe analyses are of good quality and that the minerals analysed were in equilibrium, the errors involved in thermobarometric estimates like those applied here are generally of the order of ± 25-50°C and ± 0.5-2 kbar. The microprobe analyses used for thermobarometry and representative analyses for other minerals are listed in Table 2.

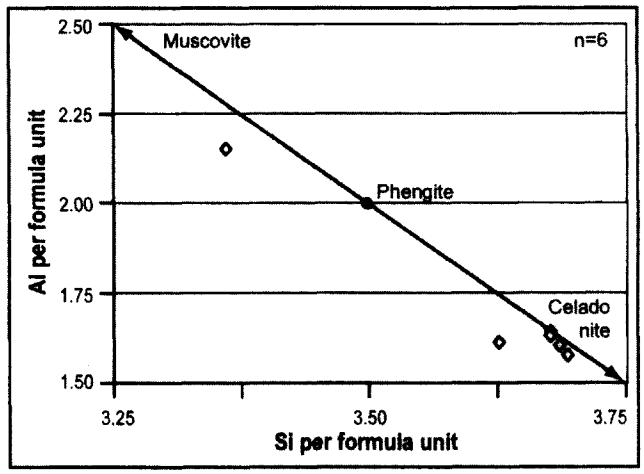

Fig. 10 - White mica compositions of phengite in metagabbro blocks.

Garnet-omphacite-phengite triplets

The Si content of white mica in phengite bearing mafic eclogites is a measure of the inverse Tschermaks substitution, replacing Al^{T1} (Al^{IV}) with Si, and the amount of Si^{T1} increases with pressure. Waters and Martin extracted thermochemical data from an internally consistent thermodynamical dataset for the equilibrium:
(pyrope + grossular + celadonite = diopside + muscovite).
The barometer was then formulated for P as a function of T and a distribution coefficient K_D. The barometer and the recommended activity models were described clearly by Carswell et al.. In this study we have applied an updated version of the barometer, that was published on the internet in 1996 (http://www.earth.ox.ac.uk/~davewa/research/ecbarcal.html). The exact formulation used here and documented in the appendix follows Waters and Martin (1996), and is henceforth referred to as WM96.

To obtain an estimate of the PT conditions, the WM96 barometer was combined with the garnet-clinopyroxene thermometer of Powell and the garnet-phengite thermometer of Green and Hellman. The temperature dependence of iron-magnesium partitioning between garnet and clinopyroxene has long been established. In this study we follow the approach of Carswell et al. and use Powell's calibration, because all analysed garnets from garnet-omphacite pairs have X_{Ca}<0.35. The distribution coefficient (K_D, for definitions see appendix) has been calculated for pairs of garnet and omphacite. Iron-magnesium partitioning between garnet and phengitic white mica is another temperature dependent exchange reaction, and was also used as a geothermometer in combination with the WM96 geobarometer.

One of our samples (MEL96-4c) contains three triplets of garnet, clinopyroxene and phengite in apparent mutual equilibrium. Analyses of these minerals in two such cases yield temperatures of about 475°C at pressures of 17.5 kbar (Table 3, Fig. 11), whilst for the third triplet slightly lower conditions of 460°C and 17.0 kbar are obtained for the equilibration of garnet, clinopyroxene and phengite (Table 3, Fig. 11). Independent support for these estimates comes from the presence of substantial amounts of rutile in the matrix as part of the high-pressure mineral assemblage, which indicates metamorphic pressures of at least 15 kbar.

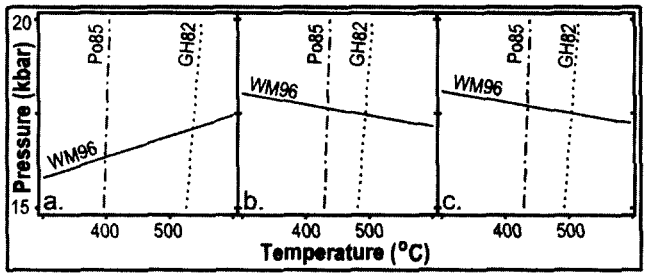

Fig. 11 - Results of garnet-clinopyroxene-phengite thermobarometry. Barometry according to Waters and Martin (1996), combined with the garnet-cpx thermometer of Powell and the garnet-phengite thermometer of Green and Hellman (cf. Carswell et al., 1997). A detailed outline of this approach is given in the appendix.

Garnet-omphacite pairs

In phengite-free eclogites WM96 cannot be used to constrain the peak metamorphic pressure. In order to obtain PT data from such phengite-free rocks the garnet-clinopyroxene thermometer has been combined with the jadeite barometer. The reactionis pressure dependent with respect to the jadeite content of omphacite. This barometer was reformulated by Carswell and Harley and is applied to several metabasic samples. Although quartz occurs only in limited quantities and has not been found to touch clinopyroxene, it seems likely that it was in equilibrium with the high-pressure assemblage. Quartz was present before and after high-pressure metamorphism, and the presence of fluids formed during prograde dehydration reactions would enhance the activity of SiO_2. Because plagioclase is not part of the high-pressure assemblage, estimates of equilibrium pressure based on the jadeite barometer are minimum estimates.

Table 4 lists the results of simultaneous solution of the garnet-clinopyroxene thermometer and the jadeite barometer with the highest PT conditions for garnet-clinopyroxene pairs of each sample. The results are a mathematical solution of the barometer for the Omp analysis with the highest jadeite content of the sample, and the thermometer applied to analyses of neighbouring pairs of Grt and Omp showing apparent (microstructural) equilibrium (see appendix).

Garnet-omphacite thermobarometry has been performed on several metagabbro samples (Table 4). The temperatures obtained range from 412 to 512°C, at minimum pressures between 10.3 and 11.9 kbar. These pressures are around 5 kbar lower than those obtained using garnet-clinopyroxene-phengite barometry. The actual equilibrium pressures of the garnet-omphacite pairs could be higher than the minimum estimates obtained here. Because the jadeite barometer yields minimum estimates only, the results are consistent with those obtained from garnet-clinopyroxene-phengite barometry, as indicated by the arrows in Figure 12. On the other hand, the jadeite content of omphacite may reflect equilibration during decompression, and therefore yield lower pressure estimates than the WM96 barometer.

Garnet-phengite pairs

The results of garnet-phengite thermometry (Green and Hellman, 1982) are listed in Table 5. The temperatures were calculated for a pressure range of 15 to 20 kbar, consistent with the pressures obtained by garnet-omphacite-phengite thermobarometry above. The obtained temperatures are 472-551°C in cases where the Si-content of phengite is high, around 442°C for intermediate phengite compositions,

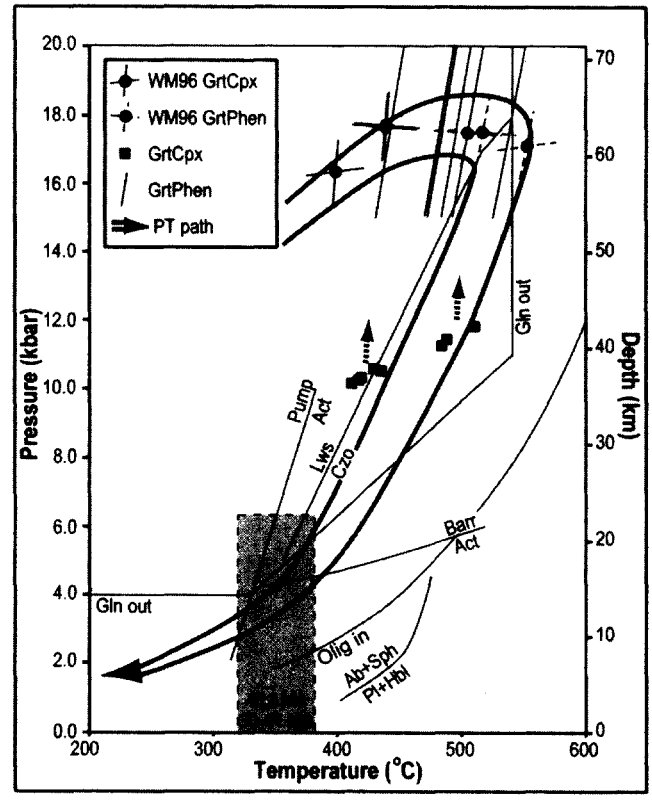

Fig. 12 - Compilation and interpretation of thermobarometric results. Thermobarometric results obtained using the different calibrations discussed in the text and the appendix. WM96GrtCpx and WM96GrtPhen are results of garnet-clinopyroxene-phengite thermobarometry. For details and references see text, Figure 11, and Table 3. GrtCpx = garnet-clinopyroxene thermometry combined with jadeite barometry, see Table 4. GrtPhen = garnet-phengite thermometry for a pressure range of 15-20 kbaer, see Table 5. Thin solid lines are reactions that constrain the metamorphic conditions. Gln-out taken from Maresch, the reaction pumpellyite + chlorite = actinolite + epidote after Liou et al., lawsonite-clinozoisite transition after Barnicoat and Fry, the lower stability limit of baroisite from Ernst, oligoclase-in reaction from Maruyama et al., and the reaction albite + titanite = plagioclase + hornblende after Moody et al. Age constraints were taken from the literature, see text for references. By 34 Ma the Voltri Massif was exposed at the Earth's surface.

Table 3 - Garnet-clinopyroxene-phengite equilibrium pressures calculated with Waters and Martin (1996, WM96) for a given temperature of 700°C.

						WM96	WM96+Po85		WM96+GH82	
Fig 11	Sample	Grt	Cpx	Phen	Si p.f.u.	P (kbar, 500 °C)	P(kbar)	T (°C)	P(kbar)	T (°C)
a	MEL96-4c	3.161	3.159	3.160	3.692	16.9	16.3	400	17.2	534
b	MEL96-4c	3.161	3.164	3.162	3.676	17.4	17.4	431	17.6	493
c	MEL96-4c	3.161	3.164	3.163	3.676	17.5	17.4	430	17.7	508

Combined graphical solution of WM96 with Powell and of WM96 with Green and Hellman. Exact formulations are in the appendix; complete microprobe analyses are in Table 2.

and around 482°C for low-Si phengite. In our reconstruction of the PT trajectory (Fig. 12) these values emerge as steep lines over a pressure range of 5 kbar.

The celadonite content of phengite can be expressed in terms of its Si content per formula unit and is dependent on pressure. The more recent calibration is an improved version, but has unfortunately not been published. The graphical representation of the 1991 calibration is included in the appendix (Fig. A1). Pressures obtained with the improved

Table 4 - Garnet-omphacite equilibrium pressures and temperatures.

Sample	Grt	Omp	Omp max Jd	core / rim	X_{Ca}	X_{Jd}	K_D	T (°C)	P (kbar)
MEL96-1B	3.108	3.107	3.105	c	0.181	0.324	28.272	417	10.3
MEL96-1E	3.16	3.17	2.80	r	0.133	0.310	14.854	485	11.3
MEL96-2B	4.56	4.55	4.64	r	0.157	0.352	14.265	512	11.9
MEL96-3A	4.75	4.74	4.72	r	0.180	0.350	17.772	489	11.5
MEL96-4B	3.32	3.33	3.30	r	0.242	0.327	32.540	436	10.6
MEL96-4c	3.161	3.164	3.159	c	0.192	0.443	27.279	431	10.6
MEL96-4d	2.29	2.28	2.28	c	0.224	0.325	31.966	427	10.4
MEL96-9A	2.100	2.103	2.102	r	0.207	0.399	31.842	419	10.4

Combined solution of Holland and Powell. Exact formulations are in the appendix; complete microprobe analyses are in Table 2.

Table 5 - Garnet-phengite equilibrium temperatures calculated with Green and Hellman for given pressures.

							GH92		Massonne 1991	
Sample	Grt	Phen	Si p.f.u.	KD	A	B	T (15 kbar, °C)	T (20 kbar, °C)	Pmin (kbar)	T (°C)
MEL96-4c	3.155	3.156	3.361	33.629	5170	4.17	470	493	9.1	442
MEL96-4c	3.161	3.160	3.692	19.687	5170	4.17	526	551	18.2	542
MEL96-4c	3.161	3.162	3.676	29.358	5170	4.17	483	507	17.3	494
MEL96-4c	3.161	3.163	3.678	26.729	5170	4.17	493	517	17.4	504
MEL96-4d	2.8	2.7	3.621	51.489	5170	4.17	431	453	15.2	432
MEL96-9A	2.99	2.96	3.684	32.675	5170	4.17	472	496	17.3	483

Combined graphical solution of Green and Hellman with Massonne. Exact formulations are in the appendix; complete microprobe analyses are in Table 2.

calibration are roughly 0.6 kbar below those obtained with the 1987 calibration. Because phengite in the metagabbros does not co-exist with K-feldspar and biotite, Massonne's barometer yields only minimum estimates of pressure (Table 5). The obtained temperatures are 483-542°C at 17.3-18.2 kbar in cases where the Si-content of phengite is high, around 432°C at 15.2 kbar for intermediate phengite compositions, and around 442°C at 9.1 kbar for low-Si phengite. Remarkably, these minimum estimates of the metamorphic pressure are consistent with those obtained using WM96 on garnet-clinopyroxene-phengite triplets, which supports the other pressure estimates, and suggests phengite is indeed part of the high-pressure assemblage.

Compilation of the PT trajectory

The PT path

Figure 12 shows a compilation of the thermobarometric results described above. In addition, reaction lines are included that constrain the evolving PT conditions on the basis of petrographical observations. A path is constructed through these results.

The PT trajectory starts at the low-temperature side of the lawsonite breakdown reaction to clinozoisite. Peak metamorphic conditions are constrained by the results of WM96 barometry, combined with the garnet-clinopyroxene and garnet-phengite thermometers. Peak metamorphic conditions are estimated to be 500 ± 50°C and 17.5 ± 0.5 kbar. Garnet-phengite pairs that were not in apparent equilibrium with clinopyroxene yielded similar temperature ranges.

Omphacite and glaucophane grew at the expense of large omphacites in pressure shadows, however, its abundant presence in the matrix, and the absence of talc from the matrix suggest that glaucophane remained stable during all of the high-pressure metamorphic evolution of these rocks. The peak metamorphic pressure is therefore loosely constrained by the terminal breakdown of glaucophane to jadeite and talc at high pressures. This reaction occurs around 30 kbar for endmember glaucophane, but Fe and Mg reduce the pressure for this reaction (Holland, 1988).

The stability of glaucophane during prograde metamorphism and the initial stages of retrogression indicates that the Gln-out reaction was not, or only slightly overstepped to higher temperature during high-pressure metamorphism (Fig. 12).

Zoning of garnet, and the recrystallisation of omphacite to form a second generation in the pressure shadows of large grains support the notion that these rocks underwent two-stage high-pressure metamorphic evolution, as was suggested by Messiga and Scambelluri (1991). The decrease of $Fe^{2+}/(Fe^{2+}+Mg)$ on garnet core-to-rim trajectories (Figure 8) indicates an increase in metamorphic temperature. There are no distinct groups of pyroxene compositions, but texturally it seems likely that the large omphacites would have compositions closer to the original igneous composition and would plot near the boundary of the aegirine-augite field, while the smaller represent the Na-richer, and higher pressure, varieties. These inferences suggest that the second generation of omphacite and the garnet rims grew closer to peak pressure and temperature conditions. After peak pressure metamorphism the rocks cooled during decompression. The pressures obtained by garnet-clinopyroxene thermobarometry using the jadeite barometer are minimum values only. It should be noted that the true equilibrium pressures may coincide with those obtained using the WM96 barometer. Alternatively, these results could be related to the initial stages of retrogression.

The retrograde history is further constrained by petrographic observations. Transformations of glaucophane to barroisite and actinolite, while no hornblende developed, suggest that the rocks had cooled below 470°C when they reached a low-pressure (P < 4 kbar) regime. The presence of clinozoisite and albite and the absence of lawsonite in the matrix indicate that the rocks did not cool below about 350°C at 5.0 kbar. The stability of the nearly-pure albite end member rather than an intermediate plagioclase lends further support to our inference that the rocks cooled from eclogite-facies peak conditions into the greenschist facies stability field, rather than into the higher-temperature amphibolite facies regime. The oligoclase-in reaction for mafic rocks hence forms an upper temperature limit to the retrograde history of the metagabbros.

Time constraints on metamorphism

Unfortunately, there are very few time constraints available for the Voltri Massif in general and for the mélange rocks addressed in this study in particular. The age of pre-Alpine rifting of the Piedmont-Ligurian oceanic basin was determined to be 150 Ma by U-Pb geochronology on zircon separates from the Beigua serpentinite unit, which is in reasonable accordance with stratigraphic data from the Briançonnais sediments suggesting an Oxfordian (ca. 160 Ma) age for breakup in the pertinent segment of the Piedmont-Ligurian realm. As rifting was followed by oceanic subduction, these ages pose an upper limit to the timing of high-pressure metamorphism. There are no geochronological data from the Voltri Massif that further constrain the onset of the high-pressure metamorphism.

K-Ar ages of white micas from gneisses of the Voltri group have yielded cooling ages of 30-41 Ma. ^{40}Ar-^{39}Ar cooling ages of white mica separates from the Beigua serpentinite unit were determined to be 45.2 ± 1.8 Ma by Dave

Rex (Unpublished data, Leeds University, 1989: Hoogerduijn Strating, pers. comm., 2000). Both of these age determinations reflect cooling below 350 ± 30°C. Additional time constraints are the stratigraphically determined Early Oligocene age of continental scree breccias, conglomerates and local lignites that were deposited on exhumed rocks of the Voltri Group, and the observation that high-pressure metamorphic clasts from the Voltri Massif occur in Oligocene sediments. It follows that the rocks of the Voltri Massif were exhumed to superficial levels by about 34 million years ago.

DISCUSSION

Comparison with previous studies

The metagabbros from the Beigua unit, from which the metagabbro blocks in the tectonic mélange were most probably derived, have been studied extensively. Their bulk chemistry indicates that they originated as MOR basalts and that they were rodingitised at or near the seafloor, before being subducted and metamorphosed at eclogite facies conditions. PT conditions during high-pressure metamorphism were previously estimated to be around 400°C at a minimum pressure of 13 kbar. The occurrence of rutile in the eclogitic mineral paragenesis, however, led Liou et al. to infer a minimum estimate for the peak pressure of 15 kbar at 475 ± 75°C. Moreover, the presence of talc as part of the high-pressure mineral assemblage in some of their samples suggests a peak metamorphic pressure of about 17 kbar, which is confirmed by the results of this study (Fig. 12).

The presence of fluid inclusions in omphacite of some deformed eclogitic metagabbros suggests that the metagabbros show a variable degree of retrogression due to the presence of fluids, enhancing localised retrograde mineral transformations.

In a paper about the retrograde PTt path of Voltri eclogites, Messiga and Scambelluri (1991) described several generations of symplectites. In one sample they found edenite/katophorite amphibole to form a symplectite (1) with plagioclase and oxides. This symplectite forms at the contacts between Grt and Cpx, and is overgrown by a later generation of glaucophane. An amphibolite facies overprint was inferred to have occurred around 550-650°C and 4 to 8 kbar. This result is questionable, because a thermobarometer was applied that was developed for assemblages where amphibole and plagioclase coexisting with epidote or zoisite (Plyusnina, 1982), neither of which is present in the symplectite. Secondly, symplectites are non-equilibrium microstructures, and the application of thermobarometric methods based on equilibrium thermodynamics is therefor problematic. Messiga and Scambelluri estimate higher peak temperatures than the upper temperature limit we have determined on the basis of the presence of nearly pure albite rather than Ca bearing plagioclase, and the continuous stability of glaucophane. The lack of any evidence for increasing temperatures during decompression, such as the growth of intermediate plagioclase or hornblende, leads us to conclude that the PT trajectory inferred in the present study (Fig. 12) is appropriate for the samples studied.

A second generation of symplectites forms at a much later stage, when glaucophane ± omphacite breaks down to for a symplectite of actinolite + albite + oxides. The authors have not derived thermobarometric estimates from this assemblage.

Although some of our samples show symplectite development around omphacite, we have not been able to constrain their relative age, and it is unclear whether these symplectites should be attributed to generation 1 or 2. As already mentioned by Messiga and Scambelluri (1991), it can be difficult to distinguish the generations because they may form in the same textural domain, at the expense of omphacite. Our samples display clear examples of type 2 symplectites, where zoned amphiboles, glaucophane cores with barroisite rims, are surrounded by an actinolite + albite symplectite.

In summary, use of a more recent barometer enabled us to estimate pressures more precisely compared with previous minimum estimates, and if the questionable high-temperature stage is omitted from Messiga and Scambelluri's (1991) curve, the resemblance to the PT trajectory in Figure 12 is striking.

Tectonic implications

The thermobarometric results from the eclogitic metagabbros addressed in this study point towards progressive cooling during exhumation. This cooling history is marked by two stages. The early stage of exhumation, from peak pressure metamorphism to greenschist facies conditions, proceeded along an effective thermal gradient of the order of 2.5-4°C/km. This value is distinctly higher than that of an adiabatic gradient, which indicates that the studied rocks were effectively cooled by the surrounding rocks during their early ascent. This stage was followed by exhumation along a gradient of some 20-25°C/km, a value close to that of a continental geotherm. There are few time constraints on the metamorphic history, but it is clear that the rocks of the Voltri Massif had arrived at the Earth's surface by the Early Oligocene. By that time, conglomerates and scree breccias were deposited on top of rocks from the Voltri Massif, and clasts of high-pressure metamorphic rocks, presumably derived from the Voltri Massif, are included in these deposits.

The tectonic setting of the Voltri Massif, located at the junction of the Alps and Apennines orogenic systems, is complicated for several reasons. First, the main tectonic units in the Voltri Massif and in the Ligurian Alps to the west have been transported to the WNW, while the Apennines east of the Voltri Massif show NNE directed nappe transport. Tectonic transport in both areas was not coeval, however, and there is evidence that in the western portions of the Apennines westerly directed transport occurred at an early stage, prior to NNE directed movements. Secondly, the Ligurian Alps, the ophiolitic Voltri Massif and Sestri-Voltaggio Zone, and the Ligurian Apennines form a relatively narrow mountain range between the Po Basin to the north and the Mediterranean to the south. The development of these major basins during Oligo-Miocene times further complicates attempts to reconstruct the orogenic geometry of the region during the early Tertiary.

The Voltri Massif and the adjacent Sestri-Voltaggio Zone to the east are made up of crustal and mantle fragments derived from the Piedmont-Ligurian ocean. During closure of this ocean, its crust and lithosphere were subducted underneath the approaching Adrian continental lithosphere. The motion of Adria is inferred to have changed from northward to NW around 35 Ma, when the Voltri Massif had already

been exhumed and was exposed at the Earth's surface. The metamorphic evolution of the eclogitic metagabbros reflects the earlier part of the convergence history, related to northward motion of Adria relative to stable Eurasia.

The current petrological study yields important information about the retrograde history of metagabbros in the Voltri Massif, but because little structural information was obtained inferences about exhumation mechanisms are not trivial. However, there appear to be two viable exhumation processes for the case of the Voltri Massif.

In recent years several groups have noted the importance of serpentinites for the exhumation of mafic eclogites in the Voltri Massif and elsewhere (e.g. Hermann et al., 2000, Guillot et al., 2000). Serpentinites often occur in the vicinity of eclogite bodies, and it is thought that their low density and viscosity may be at least partly responsible for the exhumation of eclogites, by acting as a carrier, reducing the average density, or as a lubricant. It should be noted however, that for the serpentinites need to be viscous enough to carry the dense eclogite *boudins*, and that therefor there are limits to the degree of serpentinisation, depending on the size and shape of the eclogite body transported (Guillot et al., 2001; Schwartz et al., 2001). The eclogite boulders in the serpentinite mélange were derived from the base of the Beigua serpentinite unit, which consists of about 90% serpentinite and 10 % of eclogite. Assuming that the unit was coherent enough, and the degree of serpentinisation low enough, to carry the eclogites near the base, the buoyancy of the serpentinites may indeed have played an important role in eclogite exhumation. Unfortunately the current size and shape of the eclogite boulders is probably related to development of the tectonic mélange at greenschist facies conditions (Vissers et al., 2001). Therefor the size of the eclogite bodies during most of their exhumation cannot be determined, preventing further evaluation of this exhumation mechanism for these particular rocks.

Alternatively, exhumation of the high-pressure rocks may be explained by corner flow in the orogenic wedge on top of the subduction zone as suggested by Platt. In this model, exhumation is driven by the continuous underplating of subducted material at the base of the wedge, while coeval extension in the upper portions of the wedge facilitates exhumation. This causes a material flow within the wedge bringing the deep-seated rocks towards the Earth's surface. The present peak pressure estimates point to a thickness of the pertinent orogenic wedge of at least 50 kilometres, consistent with the dimensions estimated in Platt's reconstruction of a Swiss-Italian transect of the Alps. The change in thermal gradient mentioned above, could be related to a change in movement from near-vertical at the buttress of the wedge, towards a more horizontal movement when the rocks approached the surface and were affected by extension.

Detailed structural studies have shown that the contact of the ophiolites and calcareous metasediments of the Sestri-Voltaggio Zone overlying the units of the Voltri Massif was reactivated as an extensional detachment during late Palaeocene to early Eocene deformation. These extensional structures were overprinted during compression from the Middle Eocene onward. The timing of this change in overall deformation coincides with changes in Africa-Europe convergence rates, which led Hoogerduijn Strating to suggest that the decreasing convergence rate during late Palaeocene to early Eocene times reduced the basal drag exerted on the accretionary wedge, causing it to become gravitationally unstable. The resulting extensional faults were overprinted by compressional structures when convergence accelerated again, during the Middle Eocene. Movement along extensional detachments likely contributed to the exhumation of the eclogite facies rocks of the Voltri Massif, while thrusting and concurrent erosion were possibly responsible for the final stages of exhumation, prior to its erosion, and the deposition of conglomerates and scree breccias on top of it during the Oligocene.

Our new data on the retrograde pressure temperature history of the Voltri metagabbros is consistent with both of the exhumation mechanisms discussed above. Even if structural information had been available, it would not have been possible to distinguish between exhumation driven by serpentinite buoyancy and exhumation by corner flow in the orogenic wedge, because in fact their geometries are likely to be very similar, even though the driving forces are quite different. It is not unlikely that a combination of corner flow and serpentinite buoyancy was responsible for exhumation of these mafic eclogites of the Beigua serpentinite, which are now taken up in a tectonic mélange.

CONCLUSIONS

Metagabbro blocks occur in a tectonic mélange, developed at the overthrust contact of the Beigua unit onto the Voltri-Rossiglione unit. The blocks are probably derived from the Beigua serpentinite unit and show metamorphic mineral assemblages and transformations indicating peak metamorphic conditions of 500 ± 50°C and 17.5 ± 0.5 kbar. After high-pressure metamorphism the rocks cooled during decompression. A combination of the buoyancy of the serpentinites of the Beigua unit with corner flow in the orogenic wedge on top of the subducting Piedmont-Ligurian oceanic lithosphere seems a likely cause for the exhumation of the high-pressure rocks of the Voltri Massif. Extensional faulting in response to decelerating Africa-Europe convergence probably facilitated exhumation. Exhumation was completed by around 34 million years ago, as evidenced by the deposition of Early Oligocene continental scree breccias on the rocks of the present-day Voltri Massif.

Acknowledgements

The present study was funded (in part) by the Earth and Life Sciences Foundation (ALW) of the Netherlands Organisation for Scientific Research (NWO). Electron microprobe analyses were carried out at the EU Geochemical Facility at Bristol University (UK) with funding from TMR (contract ERBFMGECT980128). Technical assistance from Dr. S.L. Kearns (Bristol), and hospitality of Dr. D. Rumble (Washington DC) are gratefully acknowledged. This paper benefited from an informal review by W. van Westrenen, and we thank M. Scambelluri for a careful and constructive review.

APPENDIX

To ensure reproducibility of the thermobarometric results of the present study all formulations that were used are explicitly given in this appendix in the form in which they were used. Definition: X_B^A = mole fraction of component B in mineral A.

1. Garnet-omphacite thermobarometry

Powell (1985)

Garnet-omphacite Fe-Mg exchange thermometer, as calibrated by Powell (1985), because X_{Ca}^{Grt} is smaller than 0.35.

$$T(K) = \frac{2790 + 10 \cdot P(kbar) + 3140 \cdot X_{Ca}^{Grt}}{1.735 + \ln K_D} \quad (1)$$

Where:

$$X_{Ca}^{Grt} = \frac{Ca}{Ca + Mg + Fe^{2+} + Mn} \quad (2)$$

And:

$$K_D = \frac{(Fe^{2+}/Mg)^{Grt}}{(Fe^{2+}/Mg)^{Cpx}} \quad (3)$$

Holland (1983)

The jadeite barometer was first calibrated by Holland and rewritten by Carswell and Harley. I used the latter calibration:

$$P - P_0(kbar) = -\frac{RT(K)}{1000 \cdot \Delta V_0} \cdot \ln\left(\frac{a_{Jd}^{Cpx} \cdot a_{SiO_2}^{Qtz}}{a_{Ab}^{Pl}}\right) \quad (4)$$

Where:

$$P_0(kbar) = 0.35 + 0.0265 \cdot T(°C) \pm 0.50 \quad (5)$$

The volume change of the reaction for high albite is

$$\Delta V_0 = -1.734 kJ/kbar = -1.734 J/bar$$

And (cpx mixing model):

$$a_{Jd}^{Cpx} = (X_{Jd}^{Cpx})^2 \cdot \gamma_{Jd}^{Cpx} \quad (6)$$

The activity coefficient of jadeite in clinopyroxene is

$$\gamma_{Jd}^{Cpx} = \exp\left(\frac{W}{RT(K)} \cdot (1 - X_{Jd}^{Cpx})^2\right) \quad (7)$$

W = 24000J/mol, R = 8.3144 J/mol·K,
And:

$$a_{SiO_2}^{Qtz} = 1$$

Because equilibrium of plagioclase with omphacite is not certain, the albite activity in plagioclase is assumed to be 1. Therefore the obtained pressures for coexisting clinopyroxene and quartz are minimum estimates.

$$a_{Ab}^{Pl} = 1$$

For simultaneous solution of the garnet-omphacite thermometer and the jadeite barometer equations (1) and (4) were combined. Define A, B and C as follows:

$$A = \frac{-R \cdot \ln((X_{Jd}^{Cpx})^2)}{1000 \cdot \Delta V_0} + 0.0265 \quad (8)$$

$$B = \frac{-R \cdot 273 \cdot \ln((X_{Jd}^{Cpx})^2) + W \cdot (1 - X_{Jd}^{Cpx})^2}{1000 \cdot \Delta V_0} - 0.35 \quad (9)$$

$$C = \frac{3140 \cdot X_{Ca}^{Grt} + 2790}{1.735 + \ln K_D} \quad (10)$$

Then:

$$T(°C) = \frac{\frac{C + 10 \cdot B}{1.735 + \ln K_D}}{1 - \frac{10 \cdot A}{1.735 + \ln K_D}} - 273 \quad (11)$$

$$P(kbar) = -\frac{R \cdot (T(°C) + 273)}{1000 \cdot \Delta V_0} \cdot \ln((X_{Jd}^{Cpx})^2) \cdot \exp\left(\frac{W}{R \cdot (T(°C) + 273) \cdot (1 - X_{Jd}^{Cpx})^2}\right) + 0.35 + 0.0265 \cdot T(°C) \quad (12)$$

again with
R = 8.3144 J/mol·K
ΔV_0 = -1.734 kJ/kbar
W = 24000 J/mol

2. Garnet-phengite thermometry

The garnet- phengite Fe-Mg exchange thermometer of Green and Hellman is defined as follows:

$$T(°C) = \frac{A + 36.0 \cdot P(kbar)}{\ln K_D + B} - 273 \quad (13)$$

Where:

$$K_D = \frac{(Fe^{2+}/Mg)^{Grt}}{(Fe^{2+}/Mg)^{Phen}} \quad (14)$$

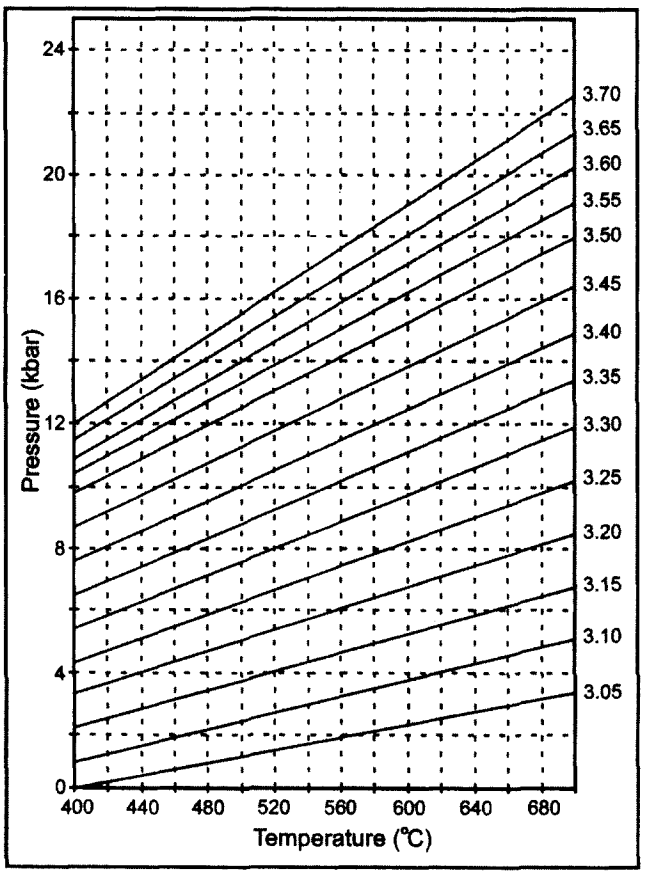

Fig. A1 - Si-isopleths for phengite in association with K-feldspar, phlogopite and quartz (redrawn and interpolated after Massonne). Minimum pressures are obtained if phengite does not coexist with K-feldspar, phlogopite and quartz. The isopleths are of Si per formula unit, on the basis of 11 oxygens.

A and B depend on the bulk composition of the rock as follows. Define

$$mg = \frac{100 \cdot MgO_{bulk}}{MgO_{bulk} + FeO_{bulk}}$$ of the bulk!

Then for pelitic (low Ca ≤ 2%) rocks with *mg* ≈ 67

A = 5560 and B = 4.65

For pelitic (low Ca ≤ 2%) rocks with *mg* = 20-30

A = 5680 and B = 4.38

For basaltic (Ca rich) rocks with *mg* ~ 67

A = 5170 and B = 4.17

3. Phengite barometry

The latest calibration of the phengite barometer (Fig. A1) was taken from Massonne. This calibration is unfortunately unpublished. Resulting pressures are about 0.6 kbar lower than with the original calibration.

4. Garnet-clinopyroxene-phengite barometry

Because of lack of an accurate barometer for mafic eclogites Waters and Martin extracted a new barometer from the internally consistent thermodynamic database of Holland and Powell (Carswell et al., 1997). The barometer is based on the inverse tschermak's substitution in phengite for triplets of garnet, omphacite and phengite in apparent equilibrium. The reaction in question is:

$$Mg_3Al_2Si_3O_{12} + 2Ca_3Al_2Si_3O_{12} + 3K(Al_1Mg_1)^{VI}Si_2^{T2}Si_2^{T1}O_{10}(OH)_2 = 6CaMgSi_2O_6 + 3KAl_2^{VI}Si_2^{T2}Si_1^{T1}Al^{T1}O_{10}(OH)_2 \quad (15)$$

(or pyrope + 2 grossular + 3 celadonite = 6 diopside + 3 muscovite, otherwise written as pyrope + 2 grossular = 6 diopside + 3 $Al_2Mg_{-2}Si_{-1}$). A revised and improved version of this barometer was published on the internet (http://www.earth.ox.ac.uk/~davewa/research/ecbarcal.html; Waters and Martin, 1996), which is the formulation that was used in the present study:

$$P(kbar) = 28.05 + 0.02044 \cdot T(K) - 0.003539 \cdot T(K) \cdot \ln K_D \quad (16)$$

The term $\ln K_D$ is a distribution coefficient, which is calculated as follows:

$$\ln K_D = 6 \cdot \ln a_{Di}^{Cpx} - \ln a_{Prp}^{Grt} - 2 \cdot \ln a_{Grs}^{Grt} + 3 \cdot \ln a_{Al_2Mg_{-1}Si_{-1}}^{Phen} \quad (17)$$

Calculation of garnet activities:

Normalise the garnet analysis to 12 oxygens and 8 cations and use simple Mg-Ca mixing. Then:

$$X_{Mg}^{Grt} = \frac{Mg}{3}$$

$$X_{Ca}^{Grt} = \frac{Ca}{3}$$

$$X_{Al}^{Grt} = \frac{Al}{2}$$

where Mg, etc represent the number of Mg cations per formula unit. Then:

$$\ln(\gamma_{Mg}^{Grt}) = \frac{(13807 - 6.276 \cdot T(K)) \cdot X_{Ca}^{Grt} \cdot (1 - X_{Mg}^{Grt})}{R \cdot T(K)}$$ and

$$\ln(\gamma_{Ca}^{Grt}) = \frac{(13807 - 6.276 \cdot T(K)) \cdot X_{Mg}^{Grt} \cdot (1 - X_{Ca}^{Grt})}{R \cdot T(K)}$$ after which:

$$\ln a_{Prp}^{Grt} = 3 \cdot \ln(X_{Mg}^{Grt}) + 3 \cdot \ln(\gamma_{Mg}^{Grt}) + 2 \cdot \ln(X_{Al}^{Grt})$$

$$\ln a_{Grs}^{Grt} = 3 \cdot \ln(X_{Ca}^{Grt}) + 3 \cdot \ln(\gamma_{Ca}^{Grt}) + 2 \cdot \ln(X_{Al}^{Grt})$$

with R = 8.314 J/mol_K

Calculation of clinopyroxene activities:

Normalise the pyroxene analysis to 6 oxygens and 4 cations and use the reciprocal salt-solution model of Holland.

$$X_{Mg,M1}^{Cpx} = Mg - cations$$

$$X_{Ca,M2}^{Cpx} = Ca - cations$$ per 6 oxygens

For long-range-disordered or Fe^{3+}-bearing pyroxenes use:

$$\ln(\gamma_{Ca,Mg}^{Cpx}) = \frac{X_{Na,M2}^{Cpx} \cdot [W_A \cdot (X_{Al,M1}^{Cpx} + X_{Fe^{3+},M1}^{Cpx}) + (W_A - W_B) \cdot X_{Fe^{2+},M1}^{Cpx}]}{R \cdot T(K)}$$

where W_A = 26000 J, and W_B = 25000 J. And then:

$$\ln a_{di} = \ln(X_{Ca,M2} \cdot X_{Mg,M1}) + \ln(\gamma_{Ca,Mg})$$

Calculation of phengite tschermak's exchange activity:

The activity expression were taken from Holland and Powell.

$$a_{Al_2Mg_{-1}Si_{-1}}^{Phen} = \frac{X_{Al,M2}^{Phen} \cdot X_{Al,T2}^{Phen}}{X_{Mg,M2}^{Phen} \cdot X_{Si,T2}^{Phen}}$$

For a microprobe analysis normalised to 11 oxygens, i.e. without taking H_2O into account, this can be expressed in terms of cations as:

$$a_{Al_2Mg_{-1}Si_{-1}}^{Phen} = \frac{(Al + Si - 4) \cdot (4 - Si)}{Mg \cdot (Si - 2)}$$

REFERENCES

Barnicoat A.C. and Fry N., 1986. High-pressure metamorphism of the Zermatt-Saas ophiolite zone, Switzerland. J. Geol. Soc. London, 143: 607-618.

Borsi L., Schärer U., Gaggero L. and Crispini L., 1996. Age, origin and geodynamic significance of plagiogranites in lherzolites and gabbros of the Piemont-Ligurian ocean basin. Earth Planet. Sci. Lett., 140: 227-241.

Capponi G., Crispini L., Cancino E. and Cavanna F., 1999. The Gargassino Valley Thrust: evidence of Oligocene-Early Miocene thrust tectonics in the Voltri Group (Ligurian Alps). Boll. Soc. Geol. It., 118: 479-484.

Carswell D.A. and Harley S.L., 1990. Mineral barometry and thermometry. In: D.A. Carswell (Ed.). Eclogite facies rocks.: p. 83-110.

Carswell D.A., O'Brien P.J., Wilson R.N. and Zhai M., 1997. Thermobarometry of phengite-bearing eclogites in the Dabie Mountains of central China. J. Metam. Geol., 15: 239-252.

Cawthorn R.G. and Collerson K.D., 1974. The recalculation of pyroxene end-member parameters and the estimation of ferrous and ferric iron content from electron microprobe analysis. Am. Mineral., 59: 1203-1208.

Chiesa S., Cortesogno L., Forcella F., Galli M., Messiga B., Pasquare G., Pedemonte G.M., Piccardo G. and Rossi P.M., 1975. Assetto strutturale ed interpretazione geodinamica del Gruppo di Voltri. Boll. Soc. Geol. It., 94: 555-581.

D'Antonio D., Gosso G., Messiga B., Scambelluri M. and Tallone S., 1984. Analisi strutturale e ricostzione litostratigrafica al margine sud-orientale del Massiccio di Voltri, zona piemon-

tese-ligure, Alpi Liguri. Mem. Soc. Geol. It., 28: 447-460.

D'Atri A., Piana F., Tallone S., Bodrato G. and Roz Gastaldi M., 1997. Tettonica Oligo-Miocena nell'Alto Monferrato (Bacino Terziario Piemontese) e nel settore nord-occidentale del Gruppo di Voltri (Asqui Terme - Cassinelle, AL). Atti Tic. Sc. Terra Serie spec., 5: 85-100.

Dercourt J., Ricou L.E. and Vrielynck B., 1993. Atlas Tethys Palaeoenvironmental maps. Gauthier-Villars, Paris, p. 307, 14 maps, 1 pl.

Dewey J.F., Helman M.L., Turco E., Hutton D.H.W. and Knott S.D., 1989. Kinematics of the western Mediterranean. In: M.P. Coward, D. Dietrich and R.G. Park (Eds.). Alpine Tectonics. Geol. Soc. Spec. Publ., 45: p. 265-283.

Droop G.T.R., 1987. A general equation for estimating Fe^{3+} concentrations in ferromagnesian silicates and oxides from microprobe analysis, using stoichiometric criteria. Mineral. Mag., 51: 431-435.

Ernst W.G., 1979. Coexisting sodic and calcic amphiboles from high-pressure metamorphic belts and the stability of barroisitic amphibole. Mineral. Mag., 43: 269-278.

Ernst W.G. and Piccardo G.B., 1979. Petrogenesis of some Ligurian peridotites - I. Mineral and bulk-rock chemistry. Geoch. Cosmoch. Acta, 43: 219-237.

Green T.H. and Hellman P.L., 1982. Fe-Mg partitioning between coexisting garnet and phengite at high pressure, and comments on a garnet-phengite geothermometer. Lithos, 15: 253-266.

Guillot S., Hattori K.H. and de Sigoyer J., 2000. Mantle wedge serpentinization and exhumation of eclogites: Insights from eastern Ladakh, northwest Himalaya. Geology, 28: 199-202.

Guillot S., Hattori K.H., de Sigoyer J., Nägler T. and Auzende A.L., 2001. Evidence of hydration of the mantle wedge and its role in the exhumation of eclogites. Earth Planet. Sci. Lett., 193: 115-127.

Haccard D. and Lorenz C., 1979. Les déformations de l'Éocène supérieur au Stampien de la terminaison septentrionale de la zone de Sestri-Voltaggio. Bull. Soc. géol. France, 21: 401-413.

Hermann J., Müntener O. and Scambelluri M., 2000. The importance of serpentinite mylonites for subduction and exhumation of oceanic crust. Tectonoph., 327: 225-238.

Holland T. and Blundy J., 1994. Non-ideal interactions in calcic amphiboles and their bearing on amphibole-plagioclase thermometry. Contrib. Mineral. Petrol., 116: 433-447.

Holland T.J.B., 1983. The experimental determination of activities in disordered and short-range ordered jadeitic pyroxenes. Contrib. Mineral. Petrol., 82: 214-220.

Holland, T.J.B., 1988. Preliminary phase relations involving glaucophane and applications to high pressure petrology: New heat capacity and thermodynamic data. Contrib. Mineral. Petrol., 99: 134-142.

Holland T.J.B. and Powell R., 1990. An enlarged and updated internally consistent thermodynamic dataset with uncertainties and correlations: the system K_2O-Na_2O-CaO-MgO-MnO-FeO-Fe_2O_3-Al_2O_3-TiO_2-SiO_2-C-H_2-O_2. J. Metam. Geol., 8: 89-124.

Hoogerduijn Strating E.H., 1991. The evolution of the Piedmont-Ligurian ocean. A structural study of ophiolite complexes in Liguria (NW Italy). Geologica Ultraiectina, 74: 144 pp.

Hoogerduijn Strating E.H., 1994. Extensional faulting in an intraoceanic subduction complex - working hypothesis for the Paleogene of the Alps-Apennine system. Tectonoph., 238: 255-273.

Hoogerduijn Strating E.H. and Van Wamel W.A., 1989. The structure of the Bracco ophiolite complex (Ligurian Appenines, Italy) - a change from Alpine to Apennine polarity. J. Geol. Soc. London, 146: 933-944.

Hunziker J.C., Desmons J. and Hurford A.J., 1992. Thirty-two years of geochronological work in the Central and Western Alps: a review on seven maps. Mémoires de Géologie (Lausanne), 13., Lausanne, 59 pp.

Kretz R., 1983. Symbols for rock-forming minerals. Am. Mineral., 68: 277-279.

Leake B.E., 1978. Nomenclature of amphiboles. Mineral. Mag., 42: 533-563.

Lemoine M., Tricart P. and Boillot G., 1987. Ultramafic and gabbroic ocean floor of the Ligurian Tethys (Alps, Corsica, Apennines): In search of a genetic model. Geology, 15: 622-625.

Lemoine M. and Trümpy R., 1987. Pre-oceanic rifting in the Alps. Tectonoph., 133: 305-320.

Liou J.G., Kim H.S. and Maruyama S., 1983. Prehnite-epidote equilibria and their petrologic applications. J. Petrol., 24: 321-342.

Liou J.G., Zhang R., Ernst W.G., Liu J. and McLimans R., 1998. Mineral parageneses in the Piampaludo eclogitic body, Gruppo di Voltri, Western Ligurian Alps. Schweiz. Mineral. Petrogr. Mitt., 78: 317-335.

Lips A.L.W., 1998. Temporal constraints on the kinematics of the destabilization of an orogen; syn- to post-orogenic extensional collapse of the Northern Aegean region. Geologica Ultraiectina, 166: 224 pp.

Lips A.L.W., White S.H. and Wijbrans J.R., 1998. $^{40}Ar/^{39}Ar$ laser-probe direct dating discrete deformational events: a continuous record of early Alpine tectonics in the Pelagonian Zone, NW Aegean area, Greece. Tectonoph., 298: 133-153.

Maresch W.V., 1977. Experimental studies on glaucophane: an analysis of present knowledge. Tectonoph., 43: 109-125.

Maruyama S., Suzuki K. and Liou J.G., 1983. Greenschist-amphibolite transition equilibria at low pressures. J. Petrol., 24: 583-604.

Massonne H.J., 1991. High-pressure, low-temperature metamorphism of pelitic and other protoliths based on experiments in the system K_2O-MgO-Al_2O_3-SiO_2-H_2O. Unpublished Post-Doc thesis, University of Bochum, 172 pp.

Massonne H.J. and Schreyer W., 1987. Phengite geobarometry based on the limiting assemblage with K-feldspar, phlogopite, and quartz. Contrib. Mineral. Petrol., 96: 212-224.

McKenzie D., 1984. The generation and compaction of partially molten rock. J. Petrol., 25: 713-765.

Messiga B., Piccardo G.B. and Ernst W.G., 1983. High-pressure eo-Alpine parageneses developed in magnesian metagabbros, Gruppo di Voltri, Western Liguria, Italy. Contrib. Mineral. Petrol., 83: 1-15.

Messiga B. and Scambelluri M., 1991. Retrograde P-T-t path for the Voltri Massif eclogites (Ligurian Alps, Italy): some tectonic implications. J. Metam. Geol., 9: 93-109.

Moody J.B., Meyer D. and Jenkins J.E., 1983. Experimental characterization of the greenschist/amphibolite boundary in mafic systems. Am. J. Sci., 283: 48-92.

Morimoto N., Ferguson A.K., Ginzburg I.V., Ross M., Seifert F.A., Zussman J., Aoki K. and Gottardi G., 1988. Nomenclature of pyroxenes. Mineral. Mag., 52: 535-550.

Morten L., Bocchio R. and Mottana A., 1985. Transformation of a superferroan eclogite within serpentinite: a case study from the Voltri Group, Italy. Chem. Geol., 50: 111-127.

Mottana A. and Bocchio R., 1975. Superferric eclogites of the Voltri Group (Pennidic Belt, Apennines). Contrib. Mineral. Petrol., 49: 201-210.

Neumann E.R., 1976. Two refinements for the calculation of structural formulae for pyroxenes and amphiboles. Norsk Geol. Tidsskr., 56: 1-6.

Nisio P. and Lardeaux J.M., 1987. Retromorphic Fe-rich talc in low-temperature eclogites: example from Monviso (Italian Western Alps). Bull. Minéral., 110: 427-437.

Piccardo G.B., Cortesogno L., Messiga B., Galli M. and Pedemonte G.M., 1977. Excursion to the metamorphic ophiolites of the Gruppo di Voltri - guide book. Rend. Soc. It. Geol. Min. Petrol., 33: 295-314.

Platt J.P., 1986. Dynamics of orogenic wedges and the uplift of high-pressure metamorphic rocks. Geol. Soc. Am. Bull., 97: 1037-1053.

Powell R., 1985. Regression diagnostics and robust regression in geothermometer/geobarometer calibration: the garnet-clinopyroxene geothermometer revisited. J. Metam. Geol., 3: 231-243.

Råheim A. and Green D.H., 1974. Experimental determination of the temperature and pressure dependence of the Fe-Mg parti-

tion coefficient for coexisting garnet and clinopyroxene. Contrib. Mineral. Petrol., 48: 179-203.

Rötzler J., Carswell D.A., Gerstenberger H. and Haase G., 1999. Transitional blueschist-epidote amphibolite facies metamorphism in the Frankenberg Massif, Germany, and geotectonic implications. J. Metam. Geol., 17: 109-125.

Schamel S. and Hunziker J., 1977. Eocene-Oligocene blueschist facies metamorphism in Liguria, Italy, and Alpine Corsica. GSA Abstr. Progr., 9: 1158-1159.

Schmid S.M. and Kissling E., 2000. The arc of the western Alps in the light of geophysical data on deep structure. Tectonics, 19: 62-85.

Schmid S.M., Pfiffner O.A., Froitzheim N., Schönborn G. and Kissling E., 1996. Geophysical-geological transect and tectonic evolution of the Swiss-Italian Alps. Tectonics, 15: 1036-1064.

Schumacher J.C., 1991. Empirical ferric iron corrections: necessity, assumptions, and effects on selected geothermobarometers. Mineral. Mag., 55: 3-18.

Schwartz S., Allemand P. and Guillot S., 2001. Numerical model of the effect of serpentinites on the exhumation of eclogitic rocks: insights from the Monviso ophiolitic massif (Western Alps). Tectonoph. 342: 193-206.

Spear F.S., 1989. Relative thermobarometry and metamorphic P-T paths. In: J.S. Daly, R.A. Cliff and B.W.D. Yardley (Eds.). Evolution of metamorphic belts. Geol. Soc. Spec. Publ., 43: p. 63-81.

Spear F.S., 1993. Metamorphic phase equilibria and pressure-temperature-time paths. Mineralogical Society of America, Washington DC, 799 pp.

Vallis F. and Scambelluri M., 1996. Redistribution of high-pressure fluids during retrograde metamorphism of eclogite-facies rocks (Voltri Massif, Italian Western Alps). Lithos, 39: 81-92.

Vissers R.L.M., Hoogerduijn Strating E.H., Heijmans M. and Krabbendam M., 2001. Structures and microstructures in a thrust-related, greenschist facies tectonic mélange, Voltri Group (NW Italy). Ofioliti 26: 33-46.

Waters D.J. and Martin H.N., 1993. Geobarometry in phengite-bearing eclogites. Terra Nova Abstr. Suppl., 5: 410-411.

Waters D.J. and Martin H.N., 1996. Geobarometry in phengite-bearing eclogites. http://www.earth.ox.ac.uk/~davewa/research/ecbarcal.html.

Williams M.L. and Grambling J.A., 1990. Manganese, ferric iron, and the equilibrium between garnet and biotite. Am. Mineral., 75: 886-908.

Received, July 2, 2001
Accepted, June 10, 2002